TRIUMF

ANNUAL REPORT
SCIENTIFIC ACTIVITIES
2000

ISSN 1492-417X

CANADA'S NATIONAL LABORATORY
FOR PARTICLE AND NUCLEAR PHYSICS

OPERATED AS A JOINT VENTURE

MEMBERS:

THE UNIVERSITY OF ALBERTA
THE UNIVERSITY OF BRITISH COLUMBIA
CARLETON UNIVERSITY
SIMON FRASER UNIVERSITY
THE UNIVERSITY OF VICTORIA

ASSOCIATE MEMBERS:

THE UNIVERSITY OF MANITOBA
L'UNIVERSITÉ DE MONTRÉAL
QUEEN'S UNIVERSITY
THE UNIVERSITY OF REGINA
THE UNIVERSITY OF TORONTO

UNDER A CONTRIBUTION FROM THE
NATIONAL RESEARCH COUNCIL OF CANADA

OCTOBER 2001

The contributions on individual experiments in this report are outlines intended to demonstrate the extent of scientific activity at TRIUMF during the past year. The outlines are not publications and often contain preliminary results not intended, or not yet ready, for publication. Material from these reports should not be reproduced or quoted without permission from the authors.

PARTICLE PHYSICS

Experiment 497
Measurement of the flavour conserving hadronic weak interaction

(J. Birchall, S.A. Page, W.T.H. van Oers, Manitoba)

The parity violation experiment [Page *et al.*, Expt. 497 (1987)] completed data-taking at 221 MeV in 1999. During the past year, Jason Bland has been working intensively on data analysis for his M.Sc. thesis (Manitoba). At the time of writing, the 1999 data set has been completely analyzed, and a reanalysis of the 1998 and 1997 data is under way to ensure that all data sets are treated in a common framework in preparation for a final publication.

The experiment is to determine the parity-violating longitudinal analyzing power in *pp* elastic scattering, $A_z = (\sigma^+ - \sigma^-)/(\sigma^+ + \sigma^-)$, where σ^+ and σ^- are the scattering cross sections for positive and negative helicity. The aim of the experiment is to measure A_z with a precision of $\pm 0.3 \times 10^{-7}$. The measurements are performed in transmission geometry, with beam energy and detector geometries selected to ensure that only parity mixing in the $^3P_2 - ^1D_2$ partial wave amplitude contributes to the measured parity violating asymmetry [Simonius, Can. J. Phys. **66**, 548 (1988)]. This amplitude has never been studied experimentally, and the possibility is unique to the energy regime accessible with the TRIUMF cyclotron. In the context of the weak meson exchange model [Desplanques *et al.*, Ann. Phys. (N.Y.) **124**, 449 (1980)], our measurement of A_z will provide a direct determination of the weak ρ-nucleon coupling constant $h_\rho^{pp} = (h_\rho^0 + h_\rho^1 + h_\rho^2/\sqrt{6})$. Recent experimental and theoretical developments confirm the importance of achieving high quality results from the TRIUMF experiment; a measurement of A_z at 13.6 MeV ($-0.93 \pm 0.20 \pm 0.05 \times 10^{-7}$) has reached the high level of accuracy reported earlier by the SIN group at 45 MeV [Eversheim *et al.*, Phys. Lett. **B256**, 11 (1991); private communication (1994); Kistryn *et al.*, Phys. Rev. Lett. **58**, 1616 (1987)].

A major effort to minimize and understand systematic error contributions is required to successfully perform an experiment to this level of precision. The first significant data set for Expt. 497 was acquired in February, 1997, with a statistical error of $\pm 0.5 \times 10^{-7}$ and most systematic errors at or below the 10^{-7} level. That result represented a major milestone for the experiment, the culmination of many years of effort to reduce both the helicity correlated beam modulations Δx_i and the sensitivities $\frac{\partial A_z}{\partial x_i}$. Data-taking continued with 3 more month-long runs during 1998 and 1999.

Beam line and instrumentation

In addition to the measuring apparatus, the TRIUMF optically pumped polarized ion source (OPPIS), cyclotron, and transport beam lines are critical components of the experimental set-up (see Fig. 1).

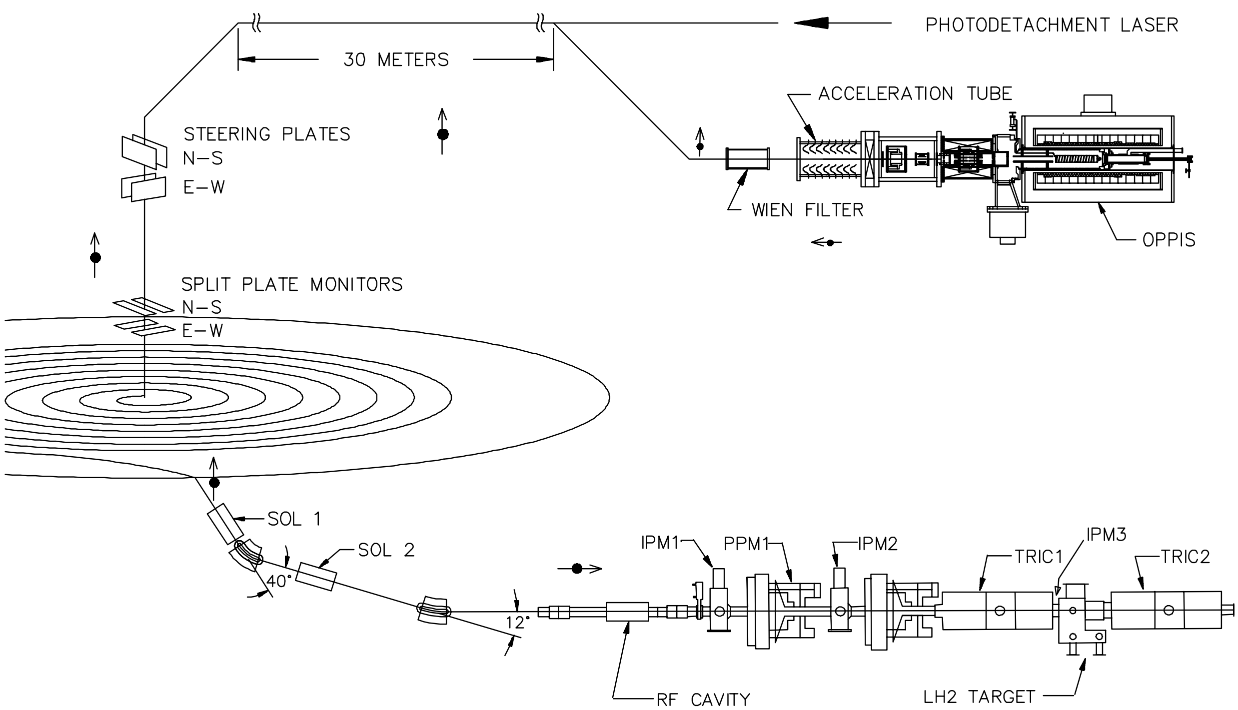

Fig. 1. General layout of TRIUMF parity experiment. (OPPIS: optically pumped polarized ion source; SOL: spin precession solenoid; IPM: intensity profile monitor; PPM: polarization profile monitor; TRIC: transverse field ionization chamber.)

A 5 μA transversely polarized beam is transported to the cyclotron through an approximately 50 m long injection beam line. The ion source Wien filter is tuned to produce vertical polarization at the entrance to the cyclotron. A 200 nA beam at 75–80% vertical polarization is extracted at 221 MeV. Spin precession through a pair of solenoid and dipole magnets results in delivery of a longitudinally polarized beam to the 40 cm long liquid hydrogen target, which scatters 4% of the beam. Note that there are two complementary states of the spin transport, so-called "positive helicity" and "negative helicity" beam line tunes, which transport spin up in the cyclotron into either + or − helicity at the parity apparatus. Half the data are acquired in each of these two beam line tune states, and consistency of the results in the two cases allows limits to be placed on systematic errors associated with the ion source alone, e.g. beam energy modulation, as discussed further below.

The custom-built parity instrumentation occupies approximately 8 m of beam line downstream between the last dipole magnet and the beam dump in the TRIUMF proton hall (beam line 4A/2). Transverse field parallel plate ion chambers TRIC1 and TRIC2 measure the beam current incident on and transmitted through the target. The parity violation signal is derived from the helicity-correlated analogue signal difference between the beam currents measured by the two TRICs. Upstream of the target are two polarization profile monitors (PPMs) to measure the distributions of transverse polarization $P_y(x)$ and $P_x(y)$ across the beam. Two intensity profile monitors (IPMs) measure the intensity distribution of beam current in x and y and are coupled to a pair of servo magnets which lock the beam path on the optimum axis through the equipment.

Major data sets

The full parity data set now consists of four major (1 month) data runs taken in February, 1997, in December, 1997–January, 1998, July–August, 1998, and May–June, 1999. These runs have a raw statistical error of approximately $\pm 0.4 \times 10^{-7}$ each. Systematic error corrections limit the precision of the overall result in all cases. A major effort has been under way to analyze the recent data sets, and preliminary results are summarized below. All but the May–June, 1999 data set have been extensively discussed in previous progress reports; a detailed analysis of the 1999 data set has been the focus of attention for the past year and is summarized in Table I.

The longitudinal analyzing power A_z is deduced from each 8-state data cycle by forming the helicity-correlated digitized TRIC difference signal, multiplied by a scale factor appropriate to the electronic and gas gains etc., and divided by the average incident beam current measured by TRIC1. Random beam and cyclotron instabilities are responsible for a large part of the width of this distribution (the normal "counting statistics" contribution is negligible), which is minimized by aligning the beam along the symmetry or "neutral axis" of the apparatus and ensuring that the two TRICs are as identical as possible in their response to the beam. Helicity-correlated changes in beam properties other than longitudinal polarization give rise to systematic errors which shift the mean of the A_z distribution away from zero; these errors are studied in a series of calibration measurements in which small spin-state-correlated modulations of beam current, energy, position, angle, and transverse polarization are purposely introduced. Interspersed data acquired in the frequent spin-off cycles provide an important zero asymmetry check of the apparatus and electronics.

Table I. Summary of the major parity data sets. χ^2/df is given for the corrected data. Each set consists of 8–10 subsets taken with alternating beam line helicity tunes. References are: 1. Hamian, Ph.D. (1998); 2. TRIUMF Annual Report (1999); 3. TRIUMF Annual Report (1999); 4. J. Bland, private communication.

Data Set	Raw A_z (10^{-7})	Corrected A_z (10^{-7})	χ^2/df
Feb. 1997[1]	1.1 ± 0.5	0.33 ± 0.65	0.5
Dec. 1997[2]	1.8 ± 0.4	0.8 ± 1.8	0.8
July 1998[3]	1.6 ± 0.3	0.9 ± 0.5	1.1
June 1999[4]	1.4 ± 0.4	1.1 ± 0.6	1.4

The dominant correction to all data sets is due to the **intrinsic** moments of transverse polarization $\langle xP_y \rangle$ and $\langle yP_x \rangle$ resulting from a non-uniform distribution of transverse polarization within the beam envelope, as distinct from the corresponding **extrinsic** polarization moments $\langle x \rangle \langle P_y \rangle$ and $\langle y \rangle \langle P_x \rangle$ which arise when a beam with finite transverse polarization is displaced from the polarization neutral axis.

The uncertainties quoted in Table I for the 4 major data sets represent a quadrature sum of statistical and systematic contributions. These are indicated separately in Table II. The statistical error includes the uncertainty in the systematic error correction ΔA_z due to the spread of the helicity correlated beam property measurements, but is dominated by the spread of the raw A_z values. The systematic error, since it is due almost entirely to the uncertainty in the intrinsic first moment sensitivities as determined from the regression analysis of the parity data, is in fact statistics dominated.

Table II. Statistical and systematic error contributions to the major parity data sets (in units of (10^{-7})). The first error is derived from the standard deviation of the corrected A_z distribution ("statistical") and the second is the contribution from the uncertainties in the sensitivity coefficients ("systematic") with first moment sensitivities derived from a regression analysis as described in the text.

Data Set	Stat.	Sys.	Corrected
Feb. 1997	0.6	0.3	0.33 ± 0.65
Dec. 1997	0.4	1.8	0.8 ± 1.8
July 1998	0.3	0.3	0.9 ± 0.5
June 1999	0.5	0.2	1.1 ± 0.6

May–June, 1999 data

Nominally, Expt. 497 ran for five weeks from 19 May, 1999 to 23 June, 1999. Unfortunately, a large number of technical failures occurred which limited the quality and quantity of the polarized data that could be acquired. The most serious problem was a failure of the ion source microwave generator, which was repaired but did not function reliably at full power for the remainder of the run, and this caused problems for the beam stability. The ion source problems were followed by a major rf spark which destroyed some high voltage components that had to be fabricated on site by the RF group, losing 5 days of beam time. Unfortunately the rf was very unstable following this repair, and this too had a major effect on the beam quality for the subsequent data-taking – the statistical variation in the asymmetry signal was erratic and on the average 20% noisier than during previous data runs. In addition, the TRIC analogue subtractor unit was subject to abnormally large time drifts of the optimum dc level for common mode signal rejection, which resulted in significant corrections for helicity correlated intensity modulation and special analysis techniques had to be applied to analyze the data, as outlined below.

Time cuts and raw data reduction

In previous data runs, the noise in the TRIC asymmetry signals was roughly constant and large bodies of data could be treated as arising from the same statistical distribution. During the May–June, 1999 run, the noise in the asymmetry signals varied by up to a factor of 2 depending upon the ion source and cyclotron conditions. A conservative approach was used to exclude anomalously noisy bursts of TRIC data from the analysis, based on determining the width of the asymmetry distribution over 50-event bundles. This resulted in a rejection of 7% of the raw data set. Subsequently, the asymmetry data were calculated as a weighted average over 1000-event bundles with the error calculated from the standard deviation of each bundle. The raw data were further reduced by placing standard cuts on the position of the beam at IPMs 1 and 2 relative to the polarization neutral axis as determined from the calibration data, as well as cuts on the average beam current, size, and the size of the intrinsic polarization moments from the PPMs, which determined the largest systematic error correction. A 20% reduction in the amount of raw data resulted from the reduction process, and the χ^2/df of the raw asymmetry data improved from 22 to 5.7, prior to correcting for systematic effects.

External calibration data

As in previous data runs, considerable beam time was devoted to calibration measurements to determine the sensitivities of the apparatus to helicity correlated position, size and polarization distributions. The latter have been extensively discussed in earlier reports; here, we illustrate the quality of the position and size modulation calibration data. Note that the size modulation data are noisier, since they are obtained with the beam position feedback loops disabled (the fast dipole steering magnets are rewired as quadrupoles and are driven in phase with the spin sequence in this case).

The false analyzing power arising from helicity correlated beam position can be written in the form

$$
\begin{aligned}
\Delta A_z &= \left(\frac{\Delta x_1 + \Delta x_2}{2}\right)(a_x x_1 + b_x x_2 + c_x) \\
&+ \left(\frac{\Delta x_1 - \Delta x_2}{2}\right)(d_x x_1 + e_x x_2 + f_x) \\
&+ \left(\frac{\Delta y_1 + \Delta y_2}{2}\right)(a_y y_1 + b_y y_2 + c_y) \\
&+ \left(\frac{\Delta y_1 - \Delta y_2}{2}\right)(d_y y_1 + e_y y_2 + f_y)\,. \quad (1)
\end{aligned}
$$

30 calibration runs were taken to find the position modulation sensitivities $(a_x.b_x...)$. Figure 2 shows two graphs of the results of the POSMOD analysis. The left graph displays measured A_z as a function of the predicted effect of position modulation as determined from the POSMOD parameter values. The right graph displays the residual from a straight line. Sensitivities were determined by MINUIT (which minimizes χ^2_ν); errors in the fitted parameters are at the $\pm 2\%$ level.

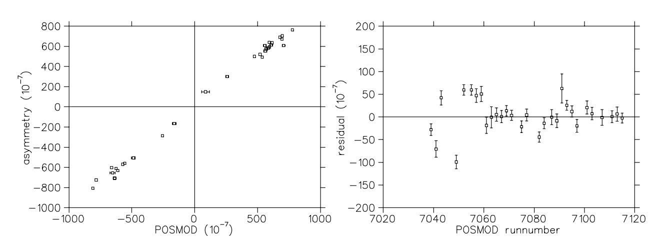

Fig. 2. (left) Measured A_z as a function of A_z predicted from position modulation, and (right) the fit residuals as a function of POSMOD run number.

The false analyzing power due to beam breathing can be expressed as:

$$\begin{aligned}\Delta A_z &= \alpha_x \sigma_{x_1} \Delta\sigma_{x_1} + \beta_x \sigma_{x_2} \Delta\sigma_{x_2} \\ &+ \alpha_y \sigma_{y_1} \Delta\sigma_{y_1} + \beta_y \sigma_{y_2} \Delta\sigma_{y_2} . \qquad (2)\end{aligned}$$

22 calibration runs were taken to determine the sensitivity of the parity apparatus to helicity correlated beam size modulation. The measured asymmetries were corrected for position modulation before the fit was carried out. Figure 3 shows the measured A_z values plotted against the A_z predicted from the position modulation fits. Errors in the fitted parameters of equation 2 are at the $\pm 5\%$ level.

Three sets of polarization neutral axis scans were taken to determine the sensitivities of the parity apparatus to components of transverse polarization. The neutral axis data were analyzed using a MINUIT fitting procedure to fit to equation 3, where ΔA_z is the TRIC signal asymmetry for transversely polarized beam, P_x and P_y are fractions of unity, and the positions $< y_1 >$ etc. are measured in mm at the locations of the two PPMs respectively:

$$\begin{aligned}\Delta A_z &= \langle P_x \rangle (a_1 \langle y_1 \rangle + a_2 \langle y_2 \rangle + a_3) \\ &+ \langle P_y \rangle (b_1 \langle x_1 \rangle + b_2 \langle x_2 \rangle + b_3) . \qquad (3)\end{aligned}$$

Fitted coefficients are in agreement with those found in previous major data sets, with error bars smaller than $\pm 1\%$.

Intrinsic first moment sensitivities

As remarked previously, the largest systematic error corrections to the parity data are those due to intrinsic first moments of polarization. The correction coefficients are most precisely determined by a regression analysis applied to the asymmetry data, as opposed to using the coefficients obtained by external calibration measurements. For the regression analysis, the input data are combined into 1000-event bundles in order to reduce the influence of the relatively large statistical uncertainties on the individual intrinsic first moment measurements from the PPMs. The bundled data are semi-corrected for all externally calibrated helicity-correlated effects, and are then analyzed to determine the intrinsic first moment sensitivities. Three different approaches were used to evaluate the intrinsic first moment sensitivities from the data. Results are in agreement in all cases with the external sensitivity scans, but with smaller error bars. The optimal sensitivities are determined to $\pm 40\%$ for $< yP_x >$ and $\pm 20\%$ for $< xP_y >$.

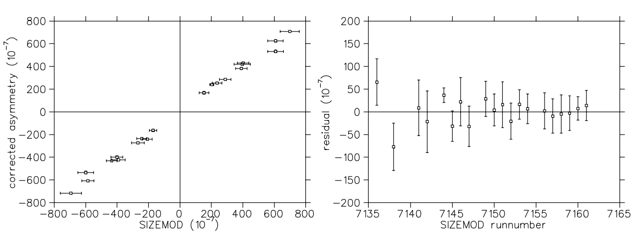

Fig. 3. (left) Corrected A_z as a function of A_z predicted from size modulation, and (right) the fit residuals as a function of SIZEMOD run number.

Helicity correlated current modulation

As noted previously, the ECR microwave tube in the ion source was not functioning properly at full power during the 1999 data run. This had the effect of introducing greater instabilities in the beam intensity than are normally experienced, and helicity-correlated current modulation was larger than usual (typically several $\times 10^{-5}$ and occasionally at the 10^{-4} level). Furthermore, the optimum dc level of the TRIC analogue subtraction unit exhibited unusually large drifts and had to be adjusted frequently during the run. These factors led to larger than usual corrections for helicity correlated current modulation, and a careful study of the sensitivities and corrections was carried out for this effect. The CIM laser which copropagates with the low energy H^- beam in the injection line provides a continuous on-line calibration of the sensitivity to current modulation. A software cut on the correction for helicity correlated current modulation was set to exclude all 2-event pairs with false effects greater than 5×10^{-7} from the data. The residual correction for $\Delta I/I$ is shown as a function of set number (alternate sets represent 2–3 days of data in different beam line helicity tunes, as noted earlier), illustrated in Fig. 4.

Reduced data set

After carrying out the analysis steps described above, a final set of cuts was applied to the data based on the absolute size of the correction to A_z on an event pair basis (recall that a minimum of 2 successive

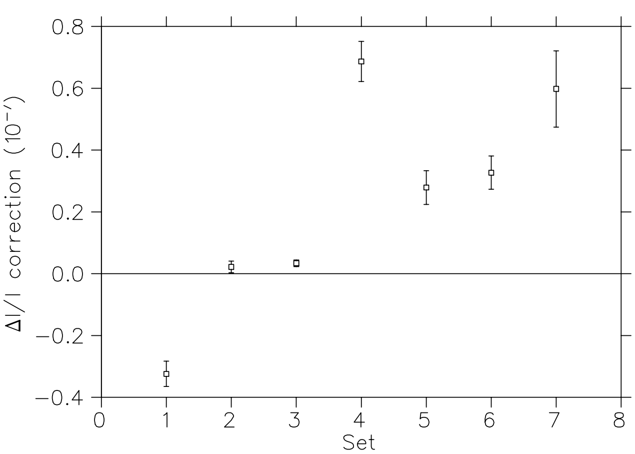

Fig. 4. $\Delta I/I$ correction as a function of set for the May, 1999 run.

$+--+-++-$ spin sequences or "events" are required to determine the polarization components and hence the corrections ΔA_z). Events were excluded with corrections more than 3 standard deviations larger than the run-averaged correction distribution. This resulted in a small reduction of the statistical uncertainty of the corrected result. Data histograms are shown in Fig. 5.

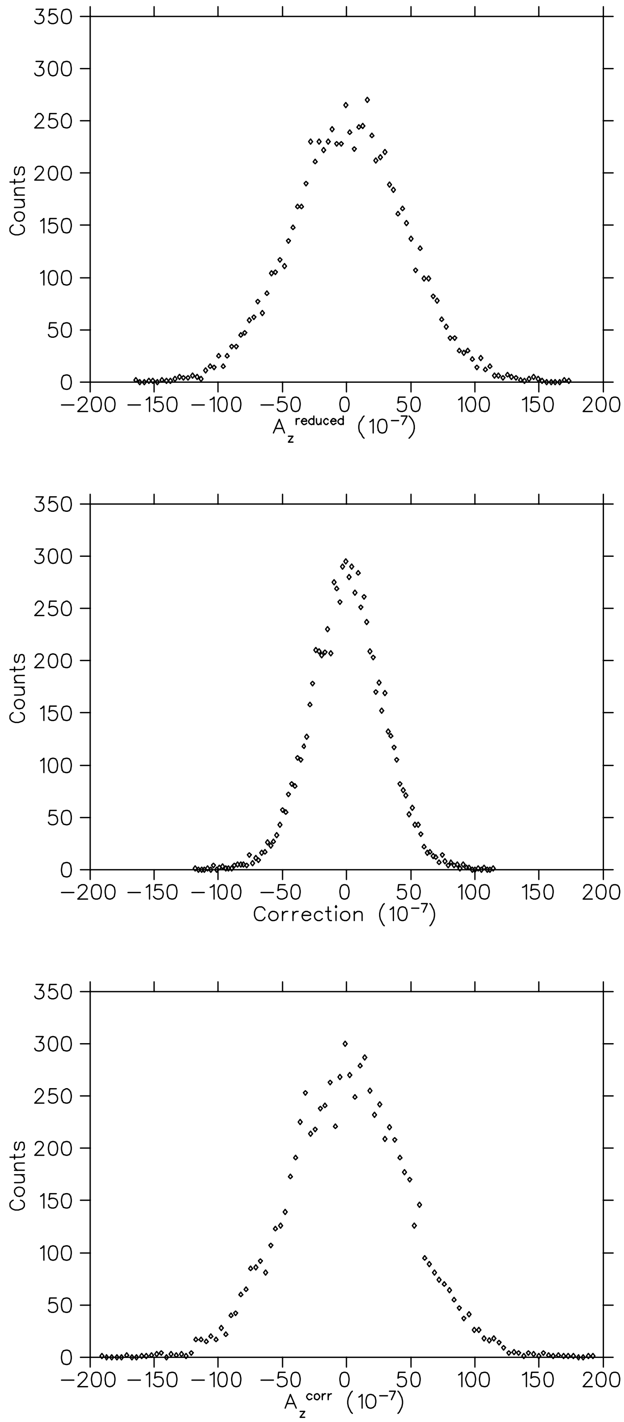

Fig. 5. (top) Histograms of A_z^{reduced}, (centre) the correction and (bottom) A_z^{corr}. Each event is a 100×2 ev bundle.

The final set of corrected A_z data for the 1999 run is shown in Table III.

Table III. Summary of final corrected data sets for the May, 1999 run. The values labelled "+" and "–" at the bottom of the table represent data for the two beam line helicity tunes respectively. Data are in very good agreement for the "+" and "–" cases.

Set	$A_z^{\mathrm{corr}}(10^{-7})$	2-events
1	$-1.17 \pm 1.27 \pm 0.46$	113,657
2	$1.36 \pm 1.03 \pm 0.27$	220,530
3	$3.72 \pm 1.26 \pm 0.34$	138,566
4	$1.30 \pm 1.23 \pm 0.16$	147,282
5	$1.13 \pm 1.72 \pm 0.20$	69,625
6	$-0.48 \pm 1.46 \pm 0.33$	95,045
7	$2.45 \pm 2.82 \pm 0.58$	24,402
Average (χ^2_ν)	$1.13 \pm 0.51 \pm 0.95$ (1.38)	809,107
+	$1.38 \pm 0.76 \pm 0.83$	346,250
–	$0.92 \pm 0.70 \pm 0.46$	462,857

Energy modulation

I4 $\delta A_z/\delta E$ calibration runs (where δE is intrinsic helicity-correlated energy modulation of the beam produced at the ion source) were conducted at interleaved periods of data-taking during the May, 1999 run. In each case, 1000 meV of artificially induced helicity-correlated energy modulation was applied to either of the spin "up" or spin "down" states. Roughly half of the data were taken in each beam line helicity tune. The EMOD calibration data were first corrected for position modulation, size modulation and intensity modulation, with $\Delta I/I$ sensitivities determined from regression analysis of the spin-on EMOD calibration run data, and then used to determine values of $\delta A_z/\delta E$. The positive helicity calibration results agree very well with each other, but unfortunately the negative helicity results are in poor agreement, necessitating an increase to our estimate of the largest possible sensitivity.

In addition to the energy modulation calibration runs, a number of measurements of the intrinsic laser-induced energy modulation in the polarized beam were taken during the acquisition of the parity data. Figure 6 illustrates the results of the intrinsic energy modulation measurements. An average δE^{eff} was calculated to be -15 ± 5 meV, where the uncertainty has been artificially enhanced by a factor of 2.5, and this was used to estimate the contribution of energy modulation to the parity data as shown in Table IV.

Table IV. Final summary of corrected helicity sets for the May, 1999 run divided into positive (346,250 event pairs) and negative (462,857 event pairs) beam line helicity. Numbers are in units of 10^{-7}.

Hel.	A_z^{reduced}	$\Delta A_z^{\mathrm{EMOD}}$	A_z^{corr}
+	3.63 ± 0.75	0.20 ± 0.08	$1.13 \pm 0.76 \pm 0.52$
–	0.13 ± 0.65	-0.09 ± 0.07	$1.01 \pm 0.70 \pm 0.34$

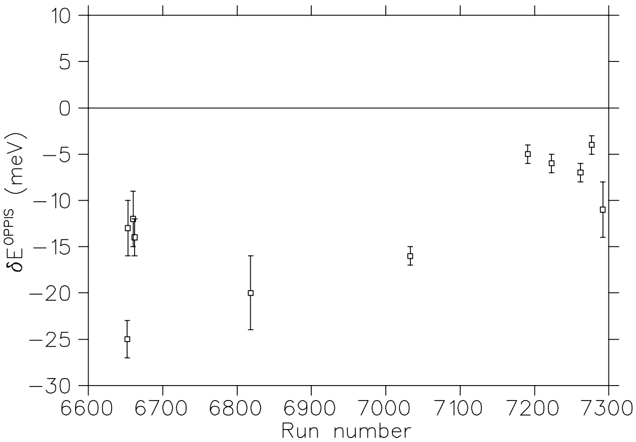

Fig. 6. The measured intrinsic energy modulation at OPPIS during the May, 1999 run.

Final result: May, 1999 data

The final result of the May, 1999 data set is $A_z^{\rm corr} = (1.1 \pm 0.5 \pm 0.2) \times 10^{-7}$. The first error bar is based on the statistical spread of the corrected A_z, while the second error bar is a quadrature sum of the systematic uncertainties for each of the measured helicity-correlated effects, including upper limits on the energy modulation correction uncertainty. The helicity correlated beam properties and individual corrections to A_z are listed in Table V.

Table V. Summary of the A_z corrections and beam properties for the May, 1999 run.

Property	Average value	$10^7 \Delta A_z$
$A_z^{\rm reduced}(10^{-7})$	1.63 ± 0.49	n/a
$y * P_x(\mu m)$	0.0 ± 0.0	-0.005 ± 0.001
$x * P_y(\mu m)$	-0.1 ± 0.0	0.069 ± 0.001
$\langle yP_x \rangle(\mu m)$	2.0 ± 0.8	0.10 ± 0.03
$\langle xP_y \rangle(\mu m)$	6.3 ± 0.9	0.64 ± 0.12
$\Delta I/I(\%)$	0.0011 ± 0.0001	0.15 ± 0.14
$\Delta\sigma_x(\mu m)$	-0.1 ± 0.1	-0.49 ± 0.03
$\Delta\sigma_y(\mu m)$	0.0 ± 0.1	0.23 ± 0.02
$\Delta x(\mu m)$	0.0 ± 0.0	0.014 ± 0.000
$\Delta y(\mu m)$	0.0 ± 0.0	-0.004 ± 0.000
Total	n/a	0.71 ± 0.21
$A_z^{\rm corr}(10^{-7})$	1.1 ± 0.5(stat)	n/a

Adding the statistical and systematic error bars in quadrature, the longitudinal analyzing power found from this analysis of the May, 1999 parity data run is $A_z = (1.1 \pm 0.6) \times 10^{-7}$, as reported in Table I.

Summary and outlook

Major progress on data analysis has been made during the past year. The last data set, taken in May-June, 1999, has now been analyzed and, by early 2001, a reanalysis of the earlier data sets making use of the same procedure should be completed. A preliminary result,

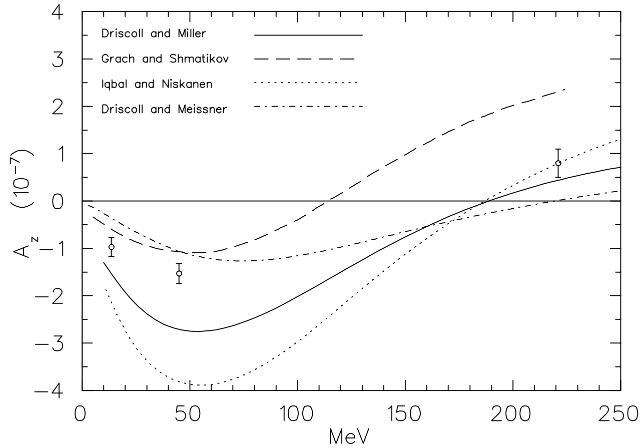

Fig. 7. Theoretical predictions for A_z in *pp* scattering, calculated by Driscoll and Miller [Phys. Rev. **C39**, 1951 (1989), *ibid.*, **C40**, 2159 (1989)] using DDH predictions for the weak meson-nucleon coupling constants; also shown are quark model calculations by Grach and Shmatikov [Phys. Lett. **B316**, 467 (1993)], meson exchange calculations by Iqbal and Niskanen [Phys. Rev. **C42**, 1872, (1990)], and a calculation by Driscoll and Meissner [Phys. Rev. **C41**, 1303 (1990)]. The highest precision existing experimental data are also shown [Eversheim *et al., op. cit.*; private communication (1994); Kistryn *et al., op. cit.*].

based on the 1997, 1998 and 1999 data sets, excluding December, 1997, is shown in Fig. 7, together with recent theoretical predictions. The existing preliminary result is $A_z = (0.8 \pm 0.3) \times 10^{-7}$. Also shown are the highest precision existing experimental data in this energy range. The TRIUMF data point supports the meson exchange prediction at the level of this first result. The final result from Expt. 497 will serve to determine uniquely for the first time an experimental constraint on the weak meson nucleon coupling constant h_ρ^{pp}.

Experiment 614
Precision measurement of the Michel parameters from muon decay
(D.R. Gill, TRIUMF; N. Rodning, Alberta)

The standard model is at present under increased scrutiny. The elevated interest is spurred primarily by the recent Kamiokande result (among others) that contradicts the usual SM input, massless neutrinos. Historically the electroweak sector of the standard model has been provided with very important input from studies of the muon's properties, its decay perhaps being the paramount characteristic. A new round of μ decay experiments, each with goals that will provide information significantly improved over their historical counterparts, are under way or about to get under way at TRIUMF, PSI and BNL. (Note reverse alphabetical order to remove bias). These new data may add support for or may produce further challenges to the standard model. Except for the presently operating g-2 experiment at BNL and the TWIST (Expt. 614) experiment that is being assembled in M13 at TRIUMF, all of these new endeavours are at PSI. This is due primarily to the considerable advantage in μ flux that PSI possesses.

The final assembly of the TWIST spectrometer, shown schematically in Fig. 8, began in 2000. This spectrometer, composed of a 2 T superconducting solenoid (originally employed for whole-body medical MRI), a set of 44 precision planar drift chambers and 12 proportional chambers, will be used to measure with high precision the differential spectrum $d^2\Gamma/dXd(cos\theta)$ of positrons from the decay $\mu^+ \rightarrow e^+\nu_e\overline{\nu}_\mu$ for polarized muons. Here, X is the positron energy ($X = 1$ corresponds to the maximum positron energy, $E_{\rm max} = 52.83$ MeV), θ is the angle between the muon spin direction and the positron momentum. The "surface" muon beam with a momentum of 29.8 MeV/c from the M13 beam line at TRIUMF will be used as the muon source. The muons will be stopped and decay at the centre, on axis, of the highly symmetrical detector system. This allows the simultaneous measurement of nearly the entire spectrum, allowing the extraction of the Michel parameters from data obtained under consistent conditions.

TWIST milestones of 2000

During 2000, TWIST began assembly of the experimental apparatus in earnest. At year's end more than half of the required drift chamber planes and almost half of the required proportional counter planes were strung. The array of drift chambers inside the spectrometer consists of 14 pairs of planes and 2 sets of 8 planes each. The former are referred to as UV modules since they measure UV (XY rotated by 45°).

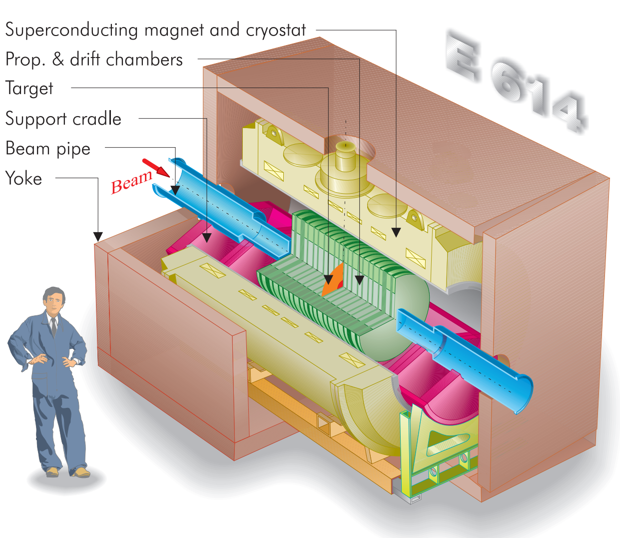

Fig. 8. The TWIST spectrometer.

Each of the 8 plane groups, also employed to measure UV, are referred to as a dense stack. The UV modules and the dense stacks are enclosed in individual gas boxes and in the final configuration will be in a helium gas envelope, 7 UV modules and a dense stack on each side of the muon stopping target. Many parts for these detectors, as well as parts for the TWIST electronics, are being made at the remote sites of the TWIST member institutions.

The accuracy of the TWIST results will be directly related to the quality of the detector. To this end special materials and special techniques are being employed in the assembly of the chambers. As well, a quality control (QC) regime is being followed as the chamber planes come off the production line. As part of the QC, the positions of the wires are measured at each end and in the centre and the tension of each wire is being determined. The high quality of the procedures being employed for the positioning and tensioning of the wires is indicated in Figs. 9–11. Figure 9 shows the typical accuracy with which the wires in a drift chamber plane are positioned, in this case at the centre of plane number 035DC. Figure 10 shows the σ of the wires across the centre of the planes as determined for 25 planes, thus the statement that Fig. 9 presents typical results. Very similar results are found for measurements of the positions at both ends of the wires, the pad end and the readout end. Figure 11 shows the results of the QC measurement of the tension of the wires for 38 drift chamber planes which have 80 wires per plane.

The experimental requirement that the drift chambers be configured into UV modules and dense stacks makes for straightforward testing of each module as it comes off the production line. In the fall, three UV modules were assembled and stacked vertically "on the bench" for testing employing cosmic rays. The results

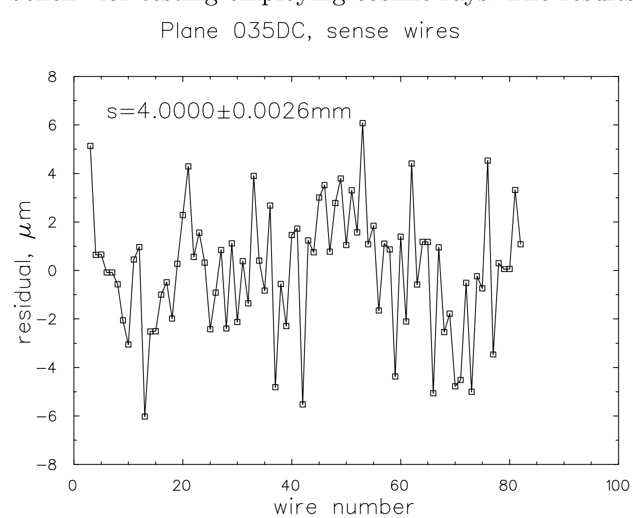

Fig. 9. A scan of wire positions across the centre of a plane. The σ of ≈3 μm is typical.

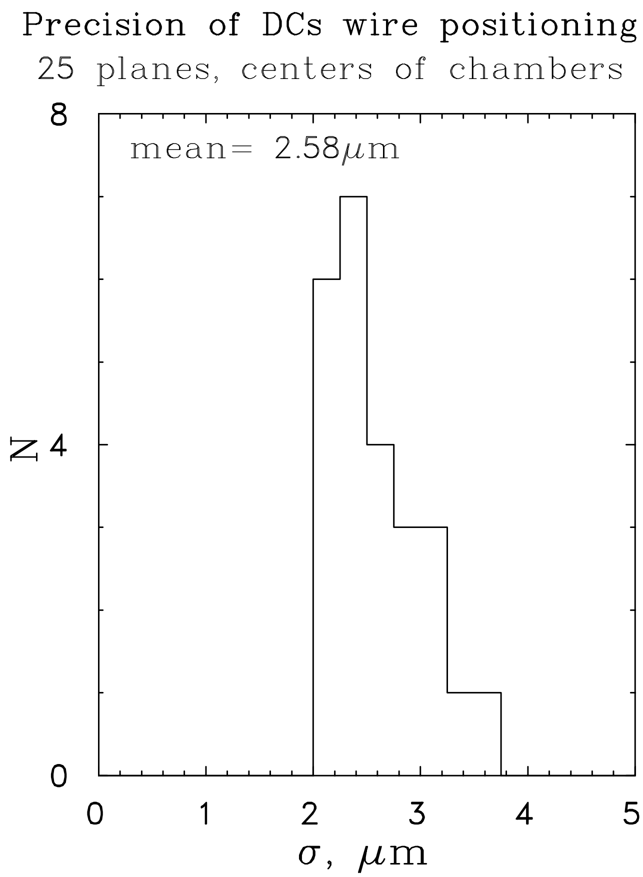

Fig. 10. The σ of wire positions for 25 planes.

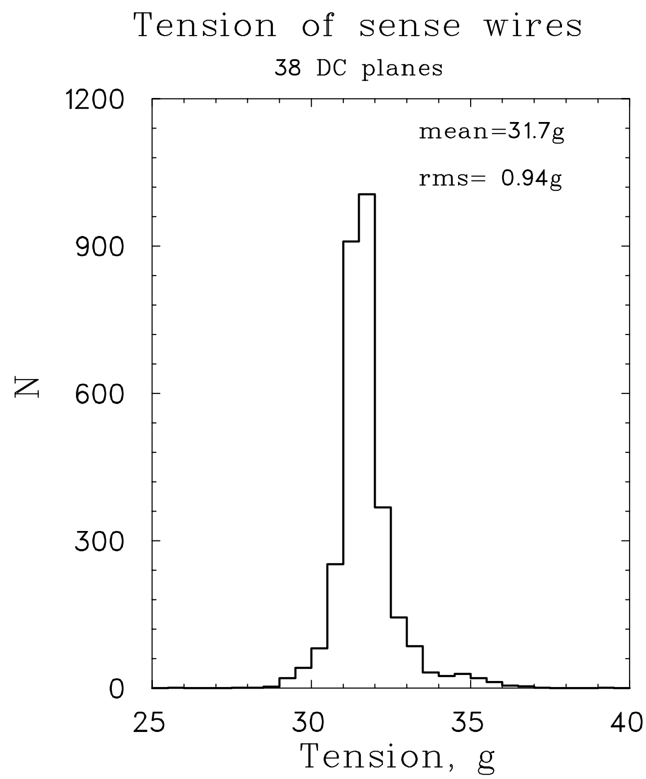

Fig. 11. The wire tensions for 38 DC planes.

of these tests indicate that the drift chambers, their electronics and the data acquisition system are performing as required. A test of the first assembled dense stack is planned for January, 2001.

The production of the required electronics, preamps and postamps, and the cabling is keeping pace with the detector production.

The steel for the magnet yoke was delivered to TRIUMF in the spring. The machining of this steel was contracted in early summer to a local firm and was completed, after several delays, and delivered to TRIUMF on December 8. TRIUMF personnel supervised the assembly of the yoke at the fabricator and it was reassembled in M13 at TRIUMF before Christmas with the solenoid in place. The commissioning and field mapping of the magnet is scheduled for early 2001.

The precision of the results of the TWIST experimental program will depend partly on the control and measurement of the M13 beam line parameters such as position, size and divergence (or emittance), momentum spread, etc. These properties of the M13 surface beam also depend on the position and profile of the proton beam when it strikes the BL1A T1 production target.

The position of the proton beam at T1 is determined using the T1 protect monitor. Studies early in 2000 showed that the sensitivity of the existing protect monitor to the horizontal position of the proton beam was not adequate for TWIST. A new protect monitor was therefore manufactured and installed for the fall running period. This new monitor has 5 mm separation between the top and bottom plates and 4 mm separation between the left and right plates. The latter have been moved in from the 5 mm separation of the original version. The protect monitor was calibrated by scanning a low intensity beam across each plate and recording the signal output. The results are dependent on the polarity of M11. Data were logged on a second by second basis and showed that the proton beam position can remain stable within $\approx$0.1 mm. These results were achieved for a beam of sufficient width that the plates were sensing the beam halo on both sides. However, for a narrow beam, for example one with a base width of 2.3 mm, it is possible for the beam to wander almost 1 mm before any halo is intercepted by the plates separated by 4 mm. This level of sensitivity may be adequate for TWIST but proton beams narrower than this could be problematic.

The stability and control of the magnetic elements of the M13 channel were monitored during a shutdown period. These studies showed the present system for monitoring the quadrupole magnets to be far from adequate for the stringent requirements of TWIST. Monitoring of quadrupole currents by a TWIST-specific system, using new current transformers, should be in place by the first running period of 2001.

Much effort has been spent by different individuals and groups to determine M13 beam parameters since installation over twenty years ago, but with the stringent TWIST requirements an opportunity to repeat and extend these measurements was taken prior to installation of the TWIST solenoid, during high intensity beam time in the fall. Many of the studies described below were made with a Be target at T1, but a limited set of data was taken with a TWIST preferred graphite target. As part of these studies a μSR apparatus was installed to examine the muon polarization vs. momentum and vs. TOF of the particles down the channel. Preliminary analysis of these measurements, assuming the surface muons are perfectly polarized, gives a polarization for the cloud muons of -0.30 ± 0.02 (where the errors of both measurements have been added in quadrature). It is interesting to note that the cloud and surface muon components of the beam have opposite polarizations.

The μSR apparatus was removed and a set of wire chambers and scintillators was installed. Measurements were then made regarding the effects of different production targets, production target alignment, and beam alignment. As well, tuning studies were performed. In particular, a set of TWIST-specific beam element settings was studied to determine if the beam profiles and emittances would be as predicted. In order to minimize the influence of multiple scattering on tuning and alignment studies, these were made with 120 MeV/c pions. With all the M13 quadrupoles turned off, scans of rates vs. position of the second slit in the central leg of M13 (F2HS) for different positions of first slit (F1HS) were used to check relative slit alignment. One of the set of maximum values was chosen such that the sum of the absolute distances of the slits from the nominal zero position was a minimum; these distances were ± 0.7 mm, i.e., nearly zero, evidence that target, dipoles and final focus are in reasonable mechanical alignment. However, when the quadrupoles were turned on, steering effects were encountered. In some cases the steering was so large that operation of the quadrupoles at their nominal values removed the beam from the active area of the XY chambers at the end of the channel. The results indicated strong horizontal steering effects from Q6 and Q7, with smaller effects in other cases. When all quads are set to nominal values, B2 requires adjustment in order to centre the beam on the first chamber at the end of the channel. The required B2 setting is 0.9% higher than that with the quadrupoles off.

The surface muon beam edge was employed to tune M13 Q2 for a horizontal dispersed focus at F1HS. This was accomplished by a scan of the F1HS position (with narrow width) for various values of Q2, the best setting being indicated by the steepest gradient in the rate as the slit is moved to higher momentum, beyond the momentum of surface muons. A contour plot is shown in Fig. 12, and the optimum value for Q2 is clearly visible.

The surface muon edge was then scanned to provide a calibration of the momentum and momentum bite of the channel. The results of several such scans, made to compare production target effects, are presented in Table VI. A scan of the positron rate near 52.83 MeV/c (the maximum for a surface positron from muon decay at rest in the production target) provides a second momentum calibration, although not as precise.

Table VI. Momentum calibration and momentum bite from momentum scans for the beryllium and graphite targets.

Beryllium target		
B1 field at edge(G)	879.6±0.4	
Momentum bite	2.1%	
Graphite target	**1st scan**	**2nd scan**
B1 field at edge(G)	878.7±0.4	878.1±0.4
Momentum bite	1.6%	1.7%

Several proposals for modifications to the beam line and its control and operation follow from the results of these studies. Some of the required improvements, such as the new current transformers for the quadrupole power supplies, are already under way. The study results have also led to suggestions for further beam studies which will be carried out in future beam periods.

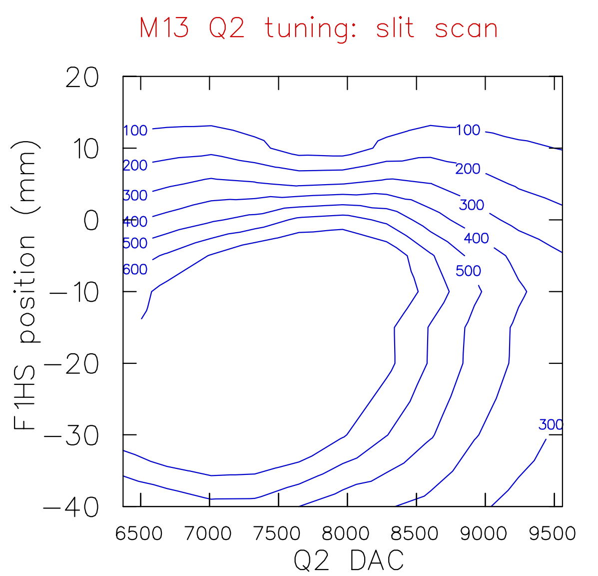

Fig. 12. Muon rate contours for a grid of settings of F1HS position and Q2 DAC. The close contour lines indicate a steep gradient at the surface muon edge, a requirement for a dispersed focus at F1.

Experiment 761
Measurement of parity violation in *pp* scattering at 221 MeV
(J. Birchall, W.T.H. van Oers, Manitoba)

Experiment 761 is a second generation parity violation experiment which aims to do a much better job of suppressing the dominant sources of systematic error – transverse polarization and current modulation – which were found in the previous experiment, Expt. 497. To this end, very high precision current mode detectors have been added to the scanning polarimeters and high resolution direct digitization of the main ion chamber signals has been adopted. Engineering runs in July/August and December were very successful and demonstrated that greatly reduced systematic uncertainty should be possible.

At the time of writing, analysis of the Expt. 497 data indicates that the parity-violating analyzing power, A_z, in the scattering of protons from hydrogen will be determined to a precision of 0.3×10^{-7}. 221 MeV is chosen because, at this energy, the $^1S_0-^3P_0$ component of A_z averages to zero over the angular acceptance of the parity equipment, leaving the $^3P_2-^1D_2$ part as the dominant contribution (see Fig. 13). This part is proportional to the weak rho meson nucleon coupling h_ρ^{pp*} alone, unlike the low energy results which are sensitive roughly equally to both h_ρ^{pp} and $h_\omega^{pp\dagger}$ –

$$\begin{aligned} A_z(45\text{ MeV}) &= 0.15h_\rho^{pp}+0.11h_\omega^{pp}, \\ A_z(221\text{ MeV}) &= -0.030h_\rho^{pp}. \end{aligned}$$

It is evident that, while it is important to measure at 221 MeV to isolate h_ρ^{pp}, a given uncertainty in A_z translates into 4 to 5 times as much uncertainty in the coupling constants as does the same A_z uncertainty at low energy; measurement at 221 MeV demands high accuracy. Although Expt. 497 has met its goal in measuring A_z, the even higher precision promised by Expt. 761 is very desirable.

At a workshop on parity violation held at ECT, the European Centre for Theoretical Studies in Nuclear Physics and Related Areas, in Trento, Italy, June 5–16, consideration was given to what are the most important calculations and experiments that should be performed in the next few years. A very strong recommendation was made to "Proceed vigorously to improve the statistical and systematic errors of the TRIUMF 221 MeV measurement to arrive at a fractional error comparable to that of the low energy results." And further, "The 221 MeV experiment *must* be completed with a most significant determination of the $^3P_2-^1D_2$ transition, which is closely related to the value of the weak rho-nucleon coupling constant."

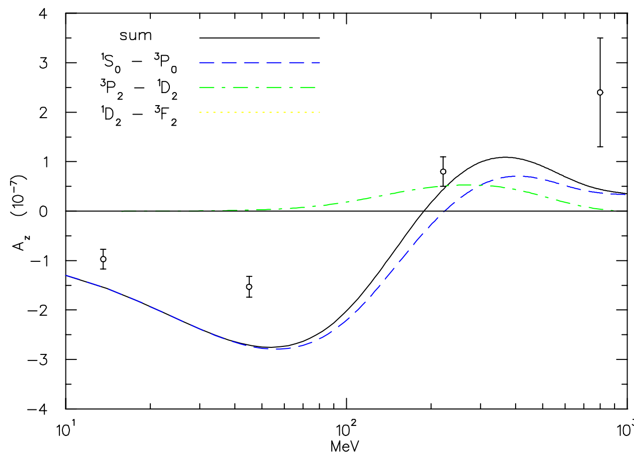

Fig. 13. $^1S_0-^3P_0$, $^3P_2-^1D_2$ and $^1D_2-^3F_2$ contributions to A_z. The calculations are by Driscoll and Miller. The TRIUMF result at 221 MeV is preliminary, based on the February, 1997, July, 1998 and June, 1999 Expt. 497 data sets. The two low energy results are from Bonn and PSI. The 800 MeV result is from LANL.

Measurement of the strangeness-conserving weak meson-nucleon coupling constants is also of interest to those investigating parity violation in electron scattering (e.g. SAMPLE, $G\emptyset$ experiments). The coupling constants are needed to calculate radiative corrections. If Expt. 761 is successful in reaching its goal, the dominant remaining uncertainty will be due to f_π.

Improvement of the measurement of A_z at 221 MeV

Polarization profile monitors

A key to an improved measurement of A_z at 221 MeV is better determination of polarization moments which are the main cause of uncertainties in systematic error corrections to A_z. This has been accomplished by using current mode polarimeters. Instead of detecting individual protons scattered from hydrogen in the polarization profile monitor (PPM) scanning CH_2 blades (counting mode operation, count-rate limited), the scattered flux of protons is measured via the integrated light output produced in large solid angle scintillators viewed by vacuum photodiodes (current mode operation). Data taken elsewhere indicated that the analyzing power for proton scattering from carbon at 225 MeV should be in excess of 0.6, even without screening out inelastic events. By adding absorbers to range out inelastic events, Expt. 761 has achieved an effective analyzing power of 0.8 for the current mode PPMs. Counting mode operation of the PPMs has been retained so that results can be compared.

Figure 14 shows the clean signals obtained from the new current mode detectors. Shown are outputs

* $h_\rho^{pp}=h_\rho^0+h_\rho^1+h_\rho^2/\sqrt{6}$
† $h_\omega^{pp}=h_\omega^0+h_\omega^1$

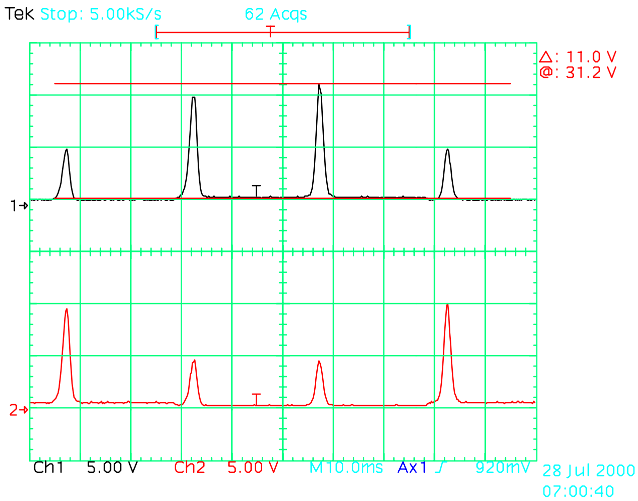

Fig. 14. Clean signals obtained from the new current mode detectors. Shown are outputs of the left and right scintillators (upper and lower traces) as the four blades of PPM1 make a single pass through the beam. The beam polarization is down, up, up and down for the four peaks in each trace. The left/right and spin up/spin down asymmetries are clearly visible.

of the left and right scintillators (upper and lower traces) as the four blades of PPM1 make a single pass through the beam. The beam polarization is down, up, up and down for the four peaks in each trace. The left/right and spin up/spin down asymmetries are clearly seen. The PPM counting time was extended in the DAQ so that background could be measured both before and after a PPM blade passed through the beam. This allows background subtraction to be performed and beam halo to be assessed much better than before. A small spin-dependence of the background is evident, which disappears when the beam is either unpolarized or polarized longitudinally at the parity apparatus. A possible effect due to the parity-allowed analyzing power, A_y, when beam scatters in the cyclotron stripping foil is not seen. The current mode detectors also work well at the PPM2 location where background might be expected to be higher.

Figure 15 shows the polarization distribution across the beam spot at PPM2 for a vertically polarized beam measured during the summer run. The upper figure shows P_y as a function of x across the beam spot in steps of 0.6 mm. The left and right detector results (short dashed lines) are from single scintillators for spin up and down normalized by beam current. The solid curve, marked “ratio”, combines left, right, spin up and down results in a ratio

$$r = \sqrt{\frac{L^+R^-}{R^+L^-}},\ P_yA_y = \frac{r-1}{r+1}$$

which is inherently less subject to systematic errors. This method has been adopted as the standard for the

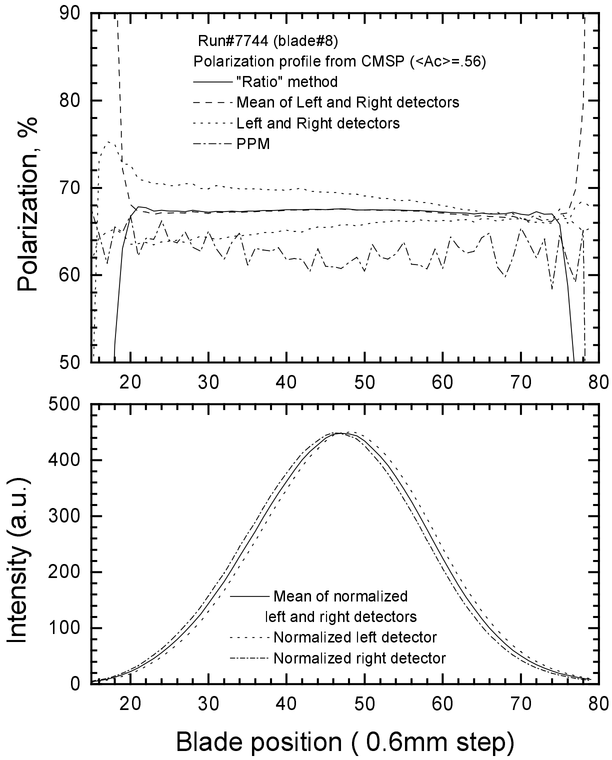

Fig. 15. The distribution of beam polarization (upper curves) and beam intensity (lower curves) across the beam spot as measured by the current-mode polarimeter at the location of PPM2.

new PPMs. Results from the counting-mode PPM are shown for comparison, marked “PPM”. The statistical spread is much larger. The lower figure shows the distribution of beam current across the beam spot, as given by the left and right current-mode scintillators. The left-right mean is used to calculate first moments of transverse polarization.

Figure 16 shows a comparison of intrinsic first moments $\langle xP_y \rangle$ measured simultaneously by counting (“old”) and current mode (“new”) polarimeters. The uncertainties of the current mode results are too small to plot. A given precision in transverse polarization and first moment was achieved in about two orders of magnitude less time than with the counting mode PPM. In other words, what took an hour, now takes a minute or less. This will be invaluable from two points of view. First, correlations of first moments with a false parity signal will be much cleaner and corrections more precise. Correction for polarization moments was the major source of systematic error in Expt. 497. The current-mode PPMs will suppress that error. Second, it is possible to explore in a much more systematic way ion source, cyclotron and beam line parameters that minimize polarization moments. Finding the source or the sources of polarization moments has been impractical so far, because many hours of running were

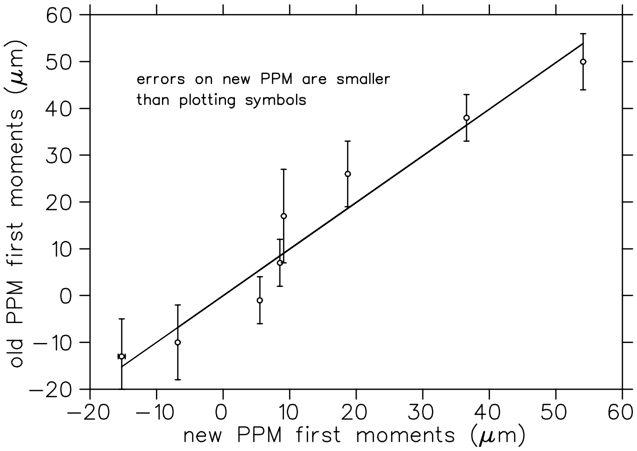

Fig. 16. Intrinsic first moments of polarization $\langle xP_y \rangle$ measured simultaneously with counting ("old") and current mode ("new") polarimeters. The two devices agree within statistics, but the new one has greatly improved precision.

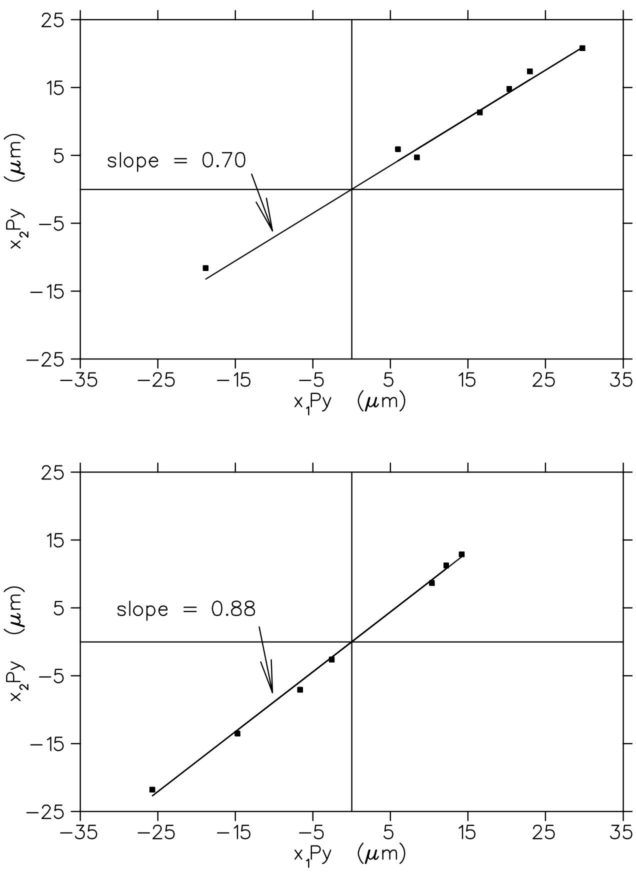

Fig. 17. First moments of transverse polarization at PPM1 and PPM2 for a wide range of cyclotron tunes (rf, main magnet, foil, ...). The difference between the top and bottom plots is the setting of the beam line magnets. It is seen that for a given beam line tune, the first moments can vary widely, but the *ratio*, $\langle xP_y \rangle_2 / \langle xP_y \rangle_1$, is essentially constant. By adjusting the beam line tune to give the "magic moment ratio", the systematic error introduced by first moments can be eliminated.

required to gain sufficient statistical precision. By use of the current mode polarimeters, we were able to very quickly study the effect of cyclotron and beam line tunes. Figure 17 shows some results from the December run. The important conclusion is that, at least to a very good approximation, the ratio of first moments at PPM1 and PPM2 is set by the beam line magnets. As cyclotron parameters change, the first moments can vary widely, but their ratio at PPM1 and PPM2 stays the same. Since the new PPMs are so fast, we can then adjust the first moment ratio to give the "magic ratio" which reduces our systematic error from first moments to zero.

Digitization of ion chamber signals

A second major improvement was in the digital subtraction of ion chamber (TRIC) signals using a new TRIUMF-designed VME digital signal averager. The previous analogue subtraction was retained for comparison. Digital subtraction has the strong advantage that it can be optimized off-line, so that the effects of current modulation can be minimized, which is the second most important source of systematic error.

Direct digitization of TRIC signals was considered for Expt. 497, but ADCs of sufficient linearity and resolution were not available at the time. Data was processed in Expt. 497 as follows. A hardware subtraction of TRIC signals was performed, the result amplified by a factor of 1000 and digitized. As the energy of the beam is 27 MeV lower at TRIC2 than at TRIC1, the TRIC2 gas pressure was lowered relative to TRIC1 to equalize ion chamber currents. A hardware gain was applied to the TRIC1 signal to minimize common-mode noise in the difference signal $1000 \times (I_2 - gI_1)$ which was digitized, where g is the hardware gain. The difference, which should be proportional to A_z, nevertheless contains a common mode (current modulation) component due to gain mismatch and nonlinearity of the ion chambers. If the current signal from TRIC2 is $I_2^{\pm} = \alpha I_1^{\pm}(1 - S(1 \pm P_z A_z))$, with $I_1^{\pm} = I_1 \pm \delta I_1$, then we can define an "analogue asymmetry",

$$\begin{aligned} \epsilon_a &= \frac{(I_2^+ - gI_1^+) - (I_2^- - gI_1^-)}{2I_1} \\ &= -S\alpha P_z A_z + \left(\alpha T - g + I_1 T \frac{d\alpha}{dI_1} \right) \frac{\delta I_1}{I_1}, \end{aligned}$$

where S is the nuclear scattering probability in the LH_2 target ($S = 0.04$) and $T = 1 - S$. α is a function of TRIC1 and TRIC2 gas gains, is nominally equal to $1/T$ and is adjusted with TRIC2 gas pressure. The hardware gain g is set by zeroing the false parity signal when the beam current is modulated by the photodetachment laser. Because of the nonlinearity term, g

must be reset if the beam current changes. Constant adjustments of g were needed during Expt. 497, partly because of electronic drifts. Note that some information is lost by digitizing the signal difference. It cannot be recovered in the data analysis so that an optimum correction cannot be applied.

When I_1 and I_2 are digitized individually, many problems disappear. The following "digital asymmetry" was formed in tests for Expt. 761:

$$\epsilon_d = \frac{I_2^+/I_1^+ - I_2^-/I_1^-}{I_2^+/I_1^+ + I_2^-/I_1^-} = -\frac{S}{T}P_z A_z + \frac{1}{\alpha}\frac{d\alpha}{dI_1}\delta I_1.$$

The gain terms are gone; only the TRIC nonlinearity term remains. A correction must now be applied for current modulation. It can be from current modulation data taken concurrently with parity data; it can be deduced from the parity data itself by applying a correction that minimizes the spread of the parity signal. In both cases, the correction is applied to the data itself, in contrast to the analogue method where the correction is applied in advance via the hardware gain, g, which may not be optimum. The digital system was first tested during the summer runs. It produced results as good as or better than the analogue system. During the December run, coherent intensity modulation data were taken and the ability to reject the intensity modulation is being analyzed.

Upgrades to data acquisition system

The parity data acquisition system was brought up to TRIUMF's currently supported standard for the summer test run. The previous system was a CAMAC/J-11 system controlled by a VAX station. Data were farmed out to two VAX stations and one ULTRIX machine for on-line analysis and data storage. The new system is shown in Fig. 18. The CAMAC

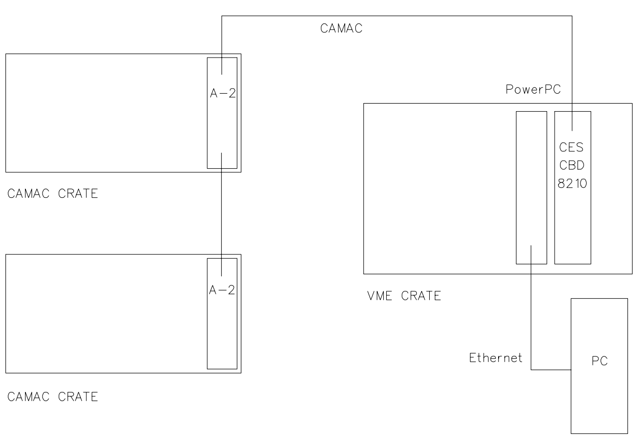

Fig. 18. Data acquisition system for Expt. 761. Existing CAMAC modules are retained. New VME modules digitize the ion chamber signals.

crates are read at a high enough rate that the J-11 incrate processors have been eliminated, their functions having been taken over by the Power PC. The three machines in the old system are replaced by one dual processor Pentium III running Linux. Most of the data acquisition and on-line analysis routines were ported to Linux in time for the test run. Further progress made during the run was impressive. Porting of software is now essentially complete, although some debugging remains, and it will be used in the 2001 running periods.

Status of optically pumped ion source

Several upgrades will be necessary to meet the demands of Expt. 761 running. Greatly increased current will be required so that sufficient beam current will be available to run ISAC at the same time as Expt. 761. To this end, TRIUMF plans to install a new Na ionizer cell which will greatly improve the beam emittance and permit much more beam to be transported to the injection line. With the greatly reduced sensitivity of Expt. 761 to transverse polarization, helicity correlated modulations of other beam properties will become much more important. This will require careful tuning of the source with all lasers and diagnostic equipment operational. Control of energy modulation will be particularly important. One TRIUMF proposal which promises to reduce all unwanted modulations is to replace the tilting etalon with a less disruptive method of shifting the frequency of the optical pumping lasers. Other planned upgrades are a new photodetachment laser for intensity modulation control measurements, and a new, more dependable power supply for the microwave generator.

Summary

The optimum energy to determine h_ρ^{pp} and h_ω^{pp} when combined with the low energy data is 221 MeV, to cancel the ${}^1S_0 - {}^3P_0$ component of A_z and to add to the data accumulated in Expt. 497. Significant improvements have been made to the parity apparatus that will allow corrections for polarization moments to be made an order of magnitude more precisely than in Expt. 497. A systematic search for sources of polarization moments is now feasible. The high resolution digitization of ion chamber signals will remove a second major source of systematic error. The collaboration is ready to start data-taking. We anticipate a short run in the summer of 2001 and a longer run in the fall.

The ATLAS experiment at the LHC

(C. Oram, TRIUMF)

As described in detail in the 1996 Annual Report, ATLAS is building a general purpose *pp* detector which is designed to exploit the full discovery potential of the Large Hadron Collider (LHC) at CERN. The TRIUMF group is responsible for the engineering of the hadronic endcap (HEC) calorimeter, and the feedthroughs for the endcap cryostat. For the HEC, this year has seen the continuation of module production and the final stages of the design of the wheel assembly equipment, while for the feedthrough project, at the University of Victoria, the project has started production, although some problems have been encountered with the batch to batch variation of low inclusion steel. This year the TRIUMF HEC group has had two visitors from China as part of its close collaboration with a Chinese group. This group is a three university cluster of Nanjing University, USTC Hefei, and Shangdong University.

Physics goals

The present theoretical understanding of elementary particles is in the context of the standard model. The standard model is a remarkably successful model, providing predictions which have been consistently confirmed by experiment for over two decades. Its agreement with experimental results, to enormous accuracy in some cases, makes it the most accurately verified model in science. Of the many elementary particles contained in the standard model, only the Higgs remains to be discovered. The central goal of ATLAS is the search for the Higgs particle.

There are good theoretical reasons to believe that the discovery of the Higgs will at least contain hints at, and more likely direct evidence of, what lies beyond the standard model. If the Higgs is composite, its existence requires as yet unknown ultra-strong forces. If it is elementary, it would be the only spinless particle to be discovered so far. There is a theoretical "naturalness" problem for the masses of spinless particles. In the standard model, which is a highly nonlinear dynamical system, the elementary particles tend to take on the heaviest of all possible mass scales which in such a model are at inaccessible energies and inconsistent with other requirements of the model. All other particles discovered thus far have natural mechanisms, such as gauge and chiral symmetries, for protecting their masses so that they can lie in the observable range. For the Higgs particle, there is no such symmetry in the present model. The only theoretical scenarios which leave the Higgs particle light enough to observe are hypothetical ones, either technicolour or supersymmetry, both radical departures from the present structure of the standard model. If Higgs is seen at LHC, one of these scenarios should be seen at the same time.

Particle theory has progressed enormously over the last few decades with many appealing scenarios for physics beyond the standard model. The most likely of these is supersymmetry and the boldest of these is superstring theory. These theories are intimately related and are both radical ideas which promise a new conceptual framework for understanding elementary particles. Though far from being complete theories so far, there are superstring models which resemble the standard model in their low energy limit. These models have a great appeal as they contain a unification of fundamental forces which includes gravity. They have already had substantial impact on gravitational physics where, for example, in addition to the long sought reconciliation of gravity with quantum mechanics, they have been used to derive a fundamental understanding of black hole thermodynamics. Superstring theory is still in its infancy, but progress has been dramatic and the promise of great things to come has captured the imagination of a substantial fraction of the world's theoretical particle physicists.

The present theoretical view is that the conventional grand unification of the strong, weak and electromagnetic forces can only work in the supersymmetric extension of the standard model. In that model, the grand unified energy scale is only two decades below the Planck scale, the ultimate energy where spacetime itself has quantum fluctuations. It is not out of the realm of imagination that, at energy scales where supersymmetry would be observed, evidence for an ultimate theory of everything, at least everything that can exist once spacetime is formed, is within human grasp.

Experiments at LHC, where the ATLAS detector will take data, will probe the energy region where the Higgs particle, possibly supersymmetry, or other structures will be visible. This will be the first experimental probe of an energy region where fundamentally new physics is expected to occur in many years. There is every reason to believe that the results will be among the most dramatic ever.

Basic ATLAS design considerations

The most prominent issue for the LHC is the quest for the origin of the spontaneous symmetry-breaking mechanism in the electroweak sector of the standard model (SM). This is related to one of the most fundamental questions of physics: What is the origin of the different particle masses? New direct experimental insight is required to answer this question.

One of the possible manifestations of the spontaneous symmetry-breaking mechanism could be the existence of a SM Higgs boson (H), or of a family of Higgs particles ($H^{\pm}$, h, H and A) when considering the minimal supersymmetric extension of the standard model

(MSSM). The Higgs search is therefore used as a first benchmark for the detector optimization. For the SM Higgs, the detector has to be sensitive to the following processes ($\ell = e$ or μ) in order to cover the full mass range above the discovery limit set by the final LEP operation in the fall of 2000:

$H \to b\bar{b}$ from WH, ZH and $t\bar{t}H$ using a $\ell^\pm$ and b-tagging,
mass range $80 < m_H < 100$ GeV;

$H \to \gamma\gamma$
mass range $90 < m_H < 150$ GeV;

$H \to WW^* \to \ell^\pm\nu\ell^\pm\nu$
mass range $150 < m_H < 200$ GeV;

$H \to ZZ^* \to 4\ell^\pm$
mass range 130 GeV $< m_H < 2m_Z$;

$H \to ZZ \to 4\ell^\pm, 2l^\pm + 2\nu$
mass range $m_H > 2m_Z$;

$H \to WW, ZZ \to l^\pm\nu + 2$ jets, $2\ell^\pm + 2$ jets from WW, ZZ fusion using tagging of forward jets for m_H up to about 1 TeV.

Here the inclusion in the above list of the decay of the Higgs to WW^* has significantly improved the sensitivity to the Higgs in the energy region around twice the mass of the Z. The sensitivity of ATLAS to the standard model Higgs is displayed in Fig. 19. The

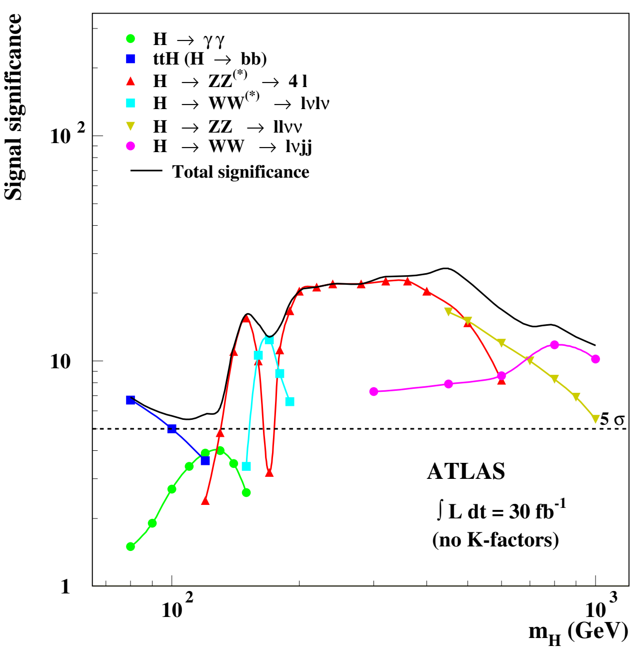

Fig. 19. Expected significance in ATLAS of the standard model Higgs boson signal, as a function of the Higgs mass, for an integrated luminosity of 10^5 pb^{-1} for several decay channels.

sensitivity improvement can be seen by comparing with the same figure in the 1999 TRIUMF Annual Report.

In addition to signatures similar to these, the MSSM Higgs searches also require sensitivity to processes such as:

$$
\begin{aligned}
A \to \tau^+\tau^- \quad & \to e\mu + \nu\text{'s} \\
& \to \ell^\pm + \text{hadrons} + \nu\text{'s}; \\
H^\pm \quad \to \tau^\pm\nu \quad & \text{from } t\bar{t} \to H^\pm W^\mp b\bar{b} \text{ and using} \\
& \ell^\pm \text{ tag and } b\text{-tagging} \\
\to 2 \text{ jets}\,.
\end{aligned}
$$

The observable cross sections for most of these processes are small over a large part of the mass range to be explored at the LHC. Hence it is important to operate at high luminosity, and to maximize the detectable rates above backgrounds by high-resolution measurements of electrons, photons, and muons.

Canada's participation in ATLAS

The Canadian group consists of 35 grant eligible physicists from TRIUMF, University of Alberta, Carleton University, UBC, University of Toronto, University of Victoria, and York University. We are strongly involved in three construction projects centred around detecting hadrons in the endcap region: the hadronic endcap project, the hadronic portion of the forward calorimeter project, and the pipeline electronics for calorimetry. In addition we are committed as part of our common project contribution to providing the feedthroughs for the two endcap cryostats. TRIUMF is directly involved in all these projects, and in the trigger and physics simulations.

The hadronic endcap project

The hadronic endcap calorimeter (HEC) is a liquid argon sampling calorimeter with copper absorbers [ATLAS Collab., ATLAS Liquid Argon Technical Design Report, December 15 (1996)]. A concise overview of this design was provided in the 1996 TRIUMF Annual Report. An artist's impression of a module can be seen in Fig. 20.

Hadronic endcap module production

This year the major scheduled milestone was the series module production of half of one wheel, and by year end production was nearly at the two-thirds mark. We are well advanced on catching up on our production schedule which was delayed by the EST board production design problem discussed in last year's Annual Report. The new design of the boards successfully passed the test beam studies in the spring. Production has been in full swing since.

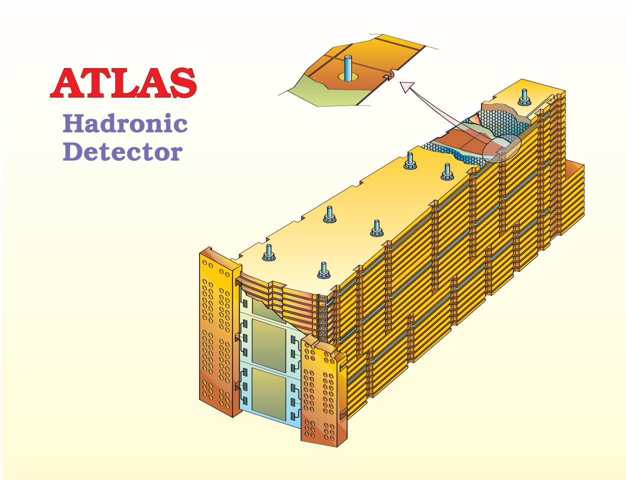

Fig. 20. Artist's impression of a hadronic endcap module.

Test beam measurements of the hadronic endcap modules

Two test beam periods on the CERN H6 beam line this year have tested the performance of the series production modules of the calorimeter. The H6 beam line provides beams from 20 to 180 GeV. Analysis of the data is on-going, and provisional results agree with the anticipated values. The resolution is the same as in previous years but the coherent noise has been reduced since the 1999 test beams. A NIM paper is in preparation. The layout of the beam line and associated systems is described in detail in the 1999 TRIUMF Annual Report.

Preparations for wheel assembly at CERN

32 modules of the HEC form a wheel. There are two wheels at each end of ATLAS, so we must construct 128 modules into four wheels. The equipment to undertake this is a Canadian responsibility. These four wheels and the two wheels of the EM calorimeter, which go in the same calorimeter, are assembled in the horizontal orientation. Hence each wheel, which weighs about 90 tonnes, must be taken from its assembly table, rotated to the vertical and moved to the cryostat. This translation and rotation of equipment is a Canadian responsibility. The engineering is being undertaken by a collaboration between Alberta and TRIUMF personnel. The project has this year entered the detailed design stage. In the spring of 2001 a production readiness review, for the stacking table and rotation/translation equipment, will be undertaken at CERN to establish that the design meets all requirements so that the project can enter the production stage.

The BaBar experiment at the Stanford Linear Accelerator Center

(C. Hearty, UBC)

Introduction

BaBar is an experiment to study the electroweak sector of particle physics using B mesons produced at the high-luminosity e^+e^- collider PEP-II. The highest-profile measurements to be performed are of the violation of the CP symmetry, which relates matter to antimatter. But BaBar will also measure sufficient parameters of the CKM matrix to determine by itself whether or not the standard model provides a consistent description of weak interactions. The high luminosity provided by PEP-II will make accessible a wide range of rare B decays, which can be sensitive to new physics both in rate and in kinematic distributions.

The first data run for BaBar started in October, 1999 and ended in September, 2000. The run – particularly the performance of PEP-II – was a tremendous success. PEP-II achieved a peak luminosity of 3.3 $\times$ 10^{33} cm^{-2}s^{-1}, 10% above design, and a total integrated value of 23.3 fb^{-1}. Backgrounds, which had been considered a potentially serious problem prior to the run, were found to be acceptable.

TRIUMF's role in BaBar was the construction of the drift chamber, one of six major detector systems. The chamber performed reliably during the run, with good tracking performance close to design value (Fig. 21). It is felt, however, that improvements to the alignment, both internal and to the other tracking system, could provide even better performance. For example, the mass resolution for reconstructing J/ψ mesons

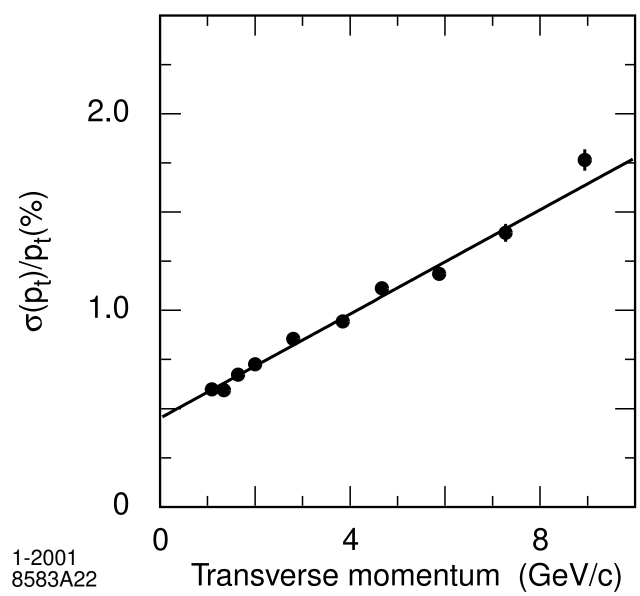

Fig. 21. Momentum resolution of the BaBar drift chamber measured using cosmic rays. $\sigma_{p_t}/p_t = 0.13\% \cdot p_t + 0.45\%$.

is currently 11.4 ± 0.3 MeV/c^2; simulations predict that resolution below 10 MeV/c^2 is possible. Another avenue being pursued is to improve the resolution when the chamber is operated at a lower voltage, 1900 V instead of 1960 V. Although not critical at the moment, a lower operating voltage would extend the eventual lifetime of the device. Canadian group members are active in both of these tracking improvements.

Measurement of $\sin 2\beta$

CP violation in the B sector is characterized by the CKM parameter $\sin 2\beta$. A non-zero value would indicate a difference in the decay rates of B^0 and $\overline{B}^0$ mesons. Based on measurements of B mixing, CP violation in K mesons, and B semi-leptonic decay rates, the expectation in the standard model is $\sin 2\beta \approx 0.70$.

The centre of mass energy of PEP-II is selected to be the mass of the $\Upsilon(4S)$ meson which decays 100% to $B\overline{B}$. Its production is approximately 25% of the total hadronic cross section. The events useful in the asymmetry analysis require a B^0 to decay to a CP eigenstate, such as $J/\psi K_S$. In order to understand what type of B decayed (i.e., B^0 or $\overline{B}^0$), the other B (called the "tag") must be partially reconstructed in a way that allows its nature to be determined. For example, the sign of the electric charge of a kaon or a high-momentum lepton is correlated with the nature of the mother B.

The correlation between the nature of the tag and signal B mesons is statistical only. Although there is one B^0 and one $\overline{B}^0$ at the instant when the first of the two decays, the remaining meson can "mix" – transform into the other type of B through higher-order box diagrams. Errors in identifying the nature of the tag meson can also dilute the relationship. The probability of error is obtained by applying the reconstruction procedure to events in which the signal B decays into fully-reconstructed final states that are not a CP eigenstate, and therefore do not have any asymmetry due to CP violation.

Of the 23 million $\Upsilon(4S)$ events produced, approximately 360 tagged signal events are measured in the final states $J/\psi K_S$ ($K_S \to \pi^+\pi^-, \pi^0\pi^0$), $\psi(2S)K_S$ ($K_S \to \pi^+\pi^-$), and $J/\psi K_L$. The asymmetry between the number of events in which the tag meson is a B^0 and the number in which it is a $\overline{B}^0$ is measured as a function of the time between the tag and signal decays to derive a value for $\sin 2\beta$. Figure 22 shows this asymmetry separately for signal events with a K_S and K_L in the final state, since these have opposite CP eigenvalues.

The result is $\sin 2\beta = 0.34 \pm 0.20(\text{stat}) \pm 0.05(\text{syst.})$. The dominant component of the systematic error is uncertainty in the parameterization of the resolution function in the time difference. (The value of the resolution is derived in the fit to the asymmetry.)

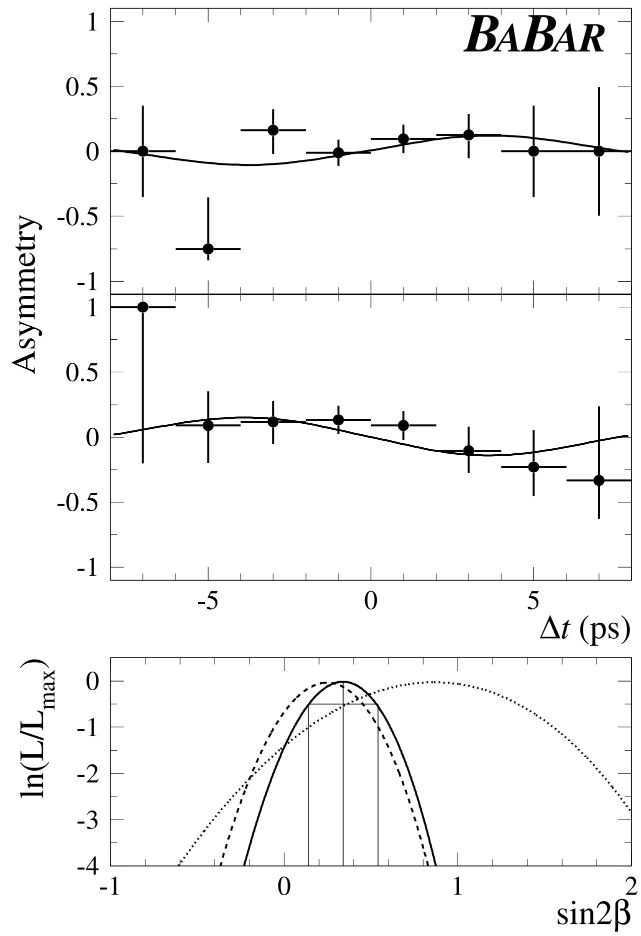

Fig. 22. The asymmetry in the number of B^0 and $\overline{B}^0$ tags as a function of Δt for (top) the $J/\psi K_S$ and $\psi(2S)K_S$ modes and (middle) the $J/\psi K_L$ mode. Bottom: variation of the log likelihood of the fit as a function of $\sin 2\beta$ for the full data set (solid line) and the subsets in (top) and (middle).

The value of $\sin 2\beta$ is somewhat low with respect to the standard model expectation and is equally consistent with no CP violation at all. The data run in 2001 is expected to more than double the integrated luminosity and help clarify the situation.

Activities of the local group

The members of BaBar local to TRIUMF have been responsible for two major analysis activities. The first is in the development of the basic event selection code used to select the events used in the CP violation analysis. More generally, this code is used to calculate the number of $\Upsilon(4S)$ events in the data set. The method starts by counting the number of events selected by the criteria and the number of muon pairs in the on-resonance data set. The same criteria are then applied to data recorded at energies slightly below the threshold for producing an $\Upsilon(4S)$. (Approximately 13% of BaBar data are recorded at this lower energy.)

The difference in the ratio of hadronic events to muon pairs at the two energies is due to $\Upsilon(4S)$ decays. The number of such events is then corrected for the efficiency of the selection to obtain the number of produced $\Upsilon(4S)$ mesons. The key features of the analysis are that the selection criteria be efficient for desired events, so that the efficiency can be calculated with low uncertainty; and that they strongly suppress beam-gas and cosmic ray events, the rate of which does not scale with the number of recorded muon pairs.

The second analysis is of "charmonium" mesons – $c\bar{c}$ states – produced in the decay of B mesons and in direct production in e^+e^- annihilation. The former has been previously observed, but BaBar will achieve significant improvements in the inclusive B branching fractions to J/ψ, $\psi(2S)$ and χ_{c1} mesons, and will make measurements of the momentum and polarization distributions of the decays.

The direct production of J/ψ mesons in e^+e^- annihilation has not previously been published. The mesons are distinguished from the far more copious production in B decays by using only those with momentum greater than is possible from a B decay, or by using the data set recorded below the $\Upsilon(4S)$ threshold (Fig. 23). The rate and angular distribution of J/ψ mesons strongly differentiate between two different approaches to QCD calculations, the "colour singlet" model and non-relativistic QCD. The latter is felt by many theorists to be a rigorous perturbative approach, while others feel it is either irrelevant at our energy or wrong. Our results strongly favour NRQCD.

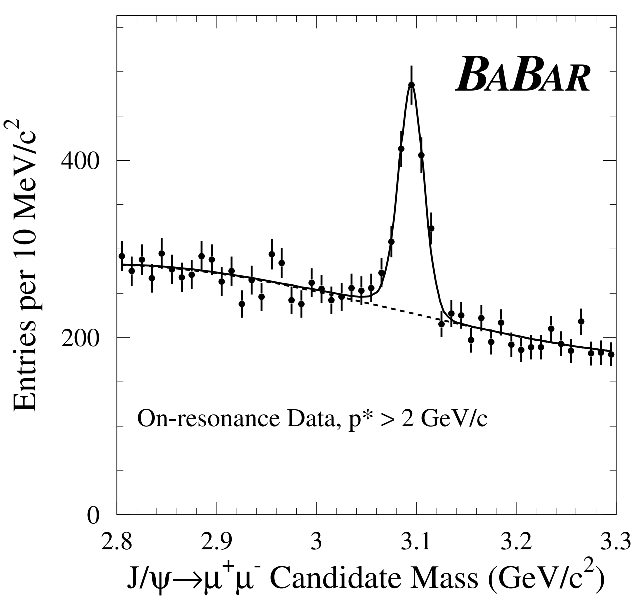

Fig. 23. Mass distribution of J/ψ candidates with momentum higher than is possible in B decays.

Our analysis also rules out the direct production of J/ψ mesons in $\Upsilon(4S)$ decay, a process that is currently listed by the particle data group with a branching fraction of (0.22 ± 0.07)%.

Outlook

The performance of the PEP-II collider has led to plans for running at luminosities above design values. Current models call for the total integrated luminosity by the end of 2004 – the fifth year of running – to be approximately 15 times the size of the first year data set. This luminosity will enable a number of precision CP violation measurements and make a wide range of rare decays accessible.

This dramatic increase in luminosity will require a substantial increase in computing power. The BaBar group, as one of several TRIUMF-based efforts, is collaborating in a consortium that is submitting a large CFI request. If successful, this would lead to a CPU farm of approximately 1000 CPUs at TRIUMF, with associated storage and networking. The facility would be used by BaBar for the production of Monte Carlo events, an area in which the BaBar collaboration is currently under-powered.

BNL 787/949
Measurement of $K^+ \to \pi^+\nu\bar{\nu}$ and other rare decays

(D. Bryman, UBC)

The ultra-rare kaon decays $K^+ \to \pi^+\nu\bar{\nu}$ and $K_L^0 \to \pi^0\nu\bar{\nu}$ offer unique access to the details of higher order phenomena associated with quark mixing and the origin of charge-parity (CP) non-invariance. Experiment 787 at the BNL AGS has presented evidence for the $K^+ \to \pi^+\nu\bar{\nu}$ decay [Adler *et al.*, Phys. Rev. Lett. **84**, 3768 (2000); Phys. Rev. Lett. **79**, 2204 (1997)] based on the observation of a single clean event. The branching ratio indicated by this observation, $1.5^{+3.4}_{-1.2} \times 10^{-10}$, is consistent with the standard model (SM) expectation. After the 1998 data set analysis is completed, the BNL 787 sensitivity for $K^+ \to \pi^+\nu\bar{\nu}$ should extend well below the most probable SM level to less than 7×10^{-11}.

Together with the proposed measurement of $K_L^0 \to \pi^0\nu\bar{\nu}$ [see BNL KOPIO, this Annual Report], a complete picture of standard model CP violation in the K system will emerge. Theoretically, these decays provide the cleanest route to the CKM parameters ρ and η. Such measurements are complementary to those to be obtained from the B system and any discrepancy in the values found would be a strong indicator of new physics.

$K^+ \to \pi^+\nu\bar{\nu}$ is a flavour-changing neutral current process, arising at the one loop level in the SM. The presence of the top quark in the loops makes this decay very sensitive to the magnitude of the elusive CKM coupling V_{td} [Buchalla and Buras, Nucl. Phys. **B400**, 225 (1993); *ibid.*, **B412**, 106 (1994); Marciano and Parsa, Phys. Rev. **D53**, R1 (1996)]. This sensitivity arises out of the hard GIM suppression which singles out the heavy t quark, the relatively small QCD corrections which have been calculated to next-to-leading-logarithmic order, and the fact that the hadronic matrix element is measured to a few per cent via an isospin transformation from $K \rightarrow \pi e \nu$ (K_{e3}) decay. Long-distance contributions are negligible so the effects of SM short-distance (vertex) physics can be clearly discerned, as well as the effects of possible non-SM physics. Overall, the branching ratio can be calculated theoretically to 5% uncertainty, most of which is due to a charm quark contribution. Using current data in the SM, the branching ratio is expected to be $\mathrm{B}(K^+ \rightarrow \pi^+ \nu \bar{\nu}) = (0.6\text{–}1.5) \times 10^{-10}$.

Most postulated new physics beyond the SM has implications for $B(K^+ \rightarrow \pi^+ \nu \bar{\nu})$ [Leurer, Phys. Rev. Lett. **71**, 1324 (1993); Davidson *et al.*, Z. Phys. **C61**, 613 (1994); Buras *et al.*, Nucl. Phys. **B520**, 3 (1998); Cho, hep-ph/9804327, KEK-TH-568 (1998); Goto *et al.*, hep-ph/9804294, KEK-TH-567 (1998); Grossman and Nir, Phys. Lett. **B398**, 163 (1997); Couture and König, Z. Phys. **C69**, 167 (1996)]. Attention has recently focused on the possible effects of a fourth generation [Hattori *et al.*, hep-ph/9804412, TOKUSHIMA-98-01 (1998)], leptoquarks, and of various forms of supersymmetry (SUSY). In the latter case, it is interesting to note that the effects of SUSY upon the K and B system generally turn out to be discernibly different.

In mid-2001, a new measurement, BNL Expt. 949, will commence. The AGS will be operated during the next several years in conjunction with the Relativistic Heavy Ion Collider (RHIC) which requires injection roughly twice per day leaving about 22 h available for AGS slow extracted beam. BNL 949 will be the primary user during the 2001–2003 period. Two years of data-taking are expected to yield a single event sensitivity of $(8\text{–}14) \times 10^{-12}$, roughly an order of magnitude below the SM prediction. In order to reach this sensitivity modest upgrades of the BNL 787 detector system are being implemented. With the completion of BNL 949, the possibility of an inconsistency with the SM prediction will be fully explored or the important top-down quark mixing parameter will be determined to a precision 15–30% if the SM expectation is confirmed.

The detection of $K^+ \rightarrow \pi^+ \nu \bar{\nu}$ (a single incident K^+ followed by the decay to a single π^+ of momentum $P < 227$ MeV/c and no other observable products) requires suppression of all backgrounds to well below the sensitivity for the signal, preferably to the level of 10^{-11}. The two most significant backgrounds are the two-body decays $K^+ \rightarrow \mu^+ \nu$ and $K^+ \rightarrow \pi^+ \pi^0$. The other significant background comes from either a π^+ in the beam scattering into the detector or from K^+ charge exchange (CEX). Careful measurement and rejection of these backgrounds which can occur at levels 10^9 to 10^{10} greater than the signal is vital.

The AGS LESB3 beam line transports 3×10^6 K^+ per 3 s spill at 700 MeV/c with a K/π ratio of 4:1 for 10^{13} protons on the production target. The K^+ are stopped in a scintillating fibre target in the centre of the detector. The fully hermetic detector is located in a 1 T solenoidal magnetic field. The central drift chamber which measures the momentum of decay products is a low-mass cylindrical chamber built at TRIUMF. The energy, range, and decay sequence of charged particles are measured in the range stack array of scintillators with two embedded layers of straw tube detectors. The range stack is instrumented with 500 MHz flash-ADC transient digitizers to measure the $\pi \rightarrow \mu \rightarrow e$ decay chain. To enhance background characterization, other elements among the beam detectors and photon veto systems are digitized by $\sim$1000 channels of 500 MHz GaAs CCDs built at TRIUMF.

The photon veto system covering 4π sr consists of a barrel assembly outside the range stack, two endcap assemblies whose main components are arrays of pure-CsI crystals, and additional systems on the beam axis both upstream and downstream of the target.

The enhancements to the BNL 787 detector for BNL 949 include new or upgraded systems in the beam instrumentation, range stack, photon veto and data acquisition. A new beam hodoscope and active degrader will improve beam tracking and photon vetoing in the beam direction. Several layers of the range stack have been replaced with brighter scintillators, and new, brighter trigger counters with better geometry have been installed. Additional radiation lengths have been added to the photon veto barrel, and other photon veto systems have been augmented or upgraded also. A new fibre-optic LED flasher system has been added to monitor range-stack and photon-veto PMTs and to assist with improving energy callibration. Many refinements to the data acquisition hardware and software have been implemented primarily to accommodate higher rates.

BNL KOPIO
Measurement of $K_L^0 \rightarrow \pi^0 \nu \bar{\nu}$ and other rare decays

(D. Bryman, UBC)

Since the discovery of CP violation in K decay in 1964, its complete understanding has been one of the most important outstanding problems in elementary particle physics. CP violation has profound implications for our picture of the relationships among the quarks and, perhaps, the leptons, as well as the origin of matter in the universe. With the advent of the standard model (SM), the primary question has revolved around establishing whether the observed CP violation was due to the complex phase in the CKM quark-mixing matrix, i.e. the existence of direct CP violation. Among all possible measurements relating to CP violation, four "golden" processes which stand out as theoretically unambiguous will allow complete elucidation of CP violation in the SM. Two are B experiments: asymmetries in $B \to \psi K_S$ decays and the ratio of B_s to B_d mixing (x_s/x_d). The other two are the branching ratios of the charged and neutral $K \to \pi\nu\overline{\nu}$ decays.

The single most incisive measurement in the study of direct CP violation will come from a measurement of the branching ratio for $K_L^0 \to \pi^0\nu\bar{\nu}$. This decay mode is unique in that it is completely dominated by direct CP violation. Within the SM $B(K_L^0 \to \pi^0\nu\bar{\nu})$ measures the area of the CKM unitarity triangles, the physical parameter that characterizes all CP violation phenomena, or the height of the triangle shown in Fig. 24. Measurements of both $B(K_L^0 \to \pi^0\nu\bar{\nu})$ and $B(K_L^+ \to \pi^+\nu\bar{\nu})$ (Expts. 787/949 at BNL [Adler *et al.*, Phys. Rev. Lett. **84**, 3768 (2000); *ibid.*, **79**, 2204 (1997)]) will allow the triangle to be reconstructed from K decay information alone.

Since theoretical uncertainties are extremely small, measurement of $B(K_L^0 \to \pi^0\nu\bar{\nu})$ will provide the standard against which all other measures of CP violation will be compared, and even small deviations from the expectation derived from SM predictions or from other measurements will unambiguously signal the presence of new physics. Using current estimates of SM parameters, $B(K_L^0 \to \pi^0\nu\bar{\nu})$ is expected to lie in the range $(3.1 \pm 1.3) \times 10^{-11}$ [Buras and Fleischer, in *Heavy Flavours II*, Buras and Linder, eds. (World Scientific, 1997), p.65; Buchalla and Buras, Nucl. Phys. **B400**, 225 (1993); *ibid.*, **B412**, 106 (1994); Marciano and Parsa, Phys. Rev. **D53**, R1 (1996)].

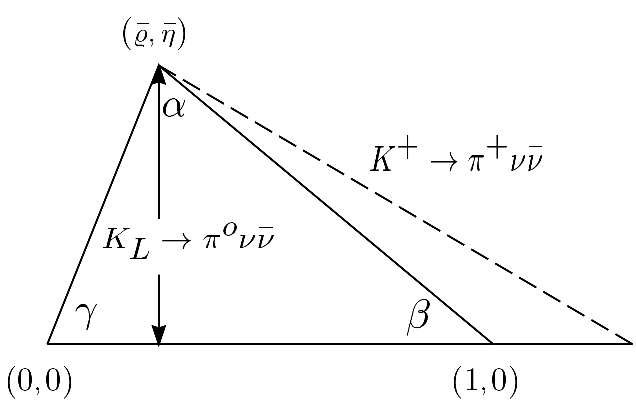

Fig. 24. The unitarity triangle.

The experiment is challenging. The decay $K_L^0 \to \pi^0\nu\bar{\nu}$ is a kinematically poorly constrained three-body decay where only a π^0 is observed, and there are competing decays also with π^0s but with branching ratios that are millions of times larger. With a 10^{-11} branching ratio, a prodigious number of kaons are required in order to achieve the desired sensitivity. The detection technique must ensure that the observed π^0 is the only observable particle from the K_L^0 decay, and provide maximum redundancy for identifying all possible backgrounds. The KOPIO experiment has been designed with these issues in mind.

The international KOPIO collaboration currently includes about a dozen institutions from Canada, the U.S.A., Japan, Russia and Switzerland. The experiment is scheduled to begin operation in 2005–6.

Measurement technique

The complete experimental signature for the $K_L^0 \to \pi^0\nu\bar{\nu}$ decay mode consists of exactly two photons with the invariant mass of a π^0, and nothing else. The experimental challenge arises from the 34% probability that a K_L^0 will emit at least one π^0 in comparison with the expected decay probability for $K_L^0 \to \pi^0\nu\bar{\nu}$ which is ten orders of magnitude smaller. Compounding the difficulty, interactions between neutrons and kaons in the neutral beam with residual gas in the decay volume can also result in emission of single π^0s, as can the decays of hyperons which might occur in the decay region.

The most important means to determine that nothing other than one π^0 was emitted in the decay is to use hermetic high sensitivity photon vetoing to eliminate any extra particles. On its own, this strategy would require an extremely high (perhaps unachievable) photon detection efficiency, and another complementary handle is needed. That handle is provided by detailed measurement of the decay kinematics in the K_L^0 centre of mass. The K_L^0 momentum is measured from time of flight (TOF) which can be obtained at the AGS in an appropriately time structured beam, and a full reconstruction of each observed photon is made through measurements of position, angle and energy. From knowledge of the decaying K_L^0 momentum, the π^0 can be transformed to the K_L^0 centre-of-mass frame and kinematic constraints can be imposed on an event-by-event basis. This technique facilitates rejection of bogus kaon decays and suppression of all other potential backgrounds.

Along with the challenge of obtaining sufficient detection sensitivity, one of the main issues in measuring an ultra-rare process is the control of systematic uncertainties in estimating tiny levels of backgrounds. The only reliable recourse is to use data to systematically study the backgrounds. This is feasible when there is enough experimental information for each event that the signal can be securely characterized, and the backgrounds confidently determined and rejected at a level well below the experiment's sensitivity.

The beam and detectors for KOPIO are based on previously established measurement techniques and new aspects have been studied in beam measurements and with prototypes and simulations. Figure 25 shows a simplified representation of the beam and detector concept. The 24 GeV primary proton beam strikes the kaon production target in 200 ps wide pulses at 25 MHz, giving a microbunch separation of 40 ns. A 500 μsr solid angle neutral beam is extracted at $\sim 40^\circ$ to produce a "soft" K_L spectrum in the range from about 0.4 GeV/c to 1.3 GeV/c. The vertical acceptance of the beam (0.005 r) is much smaller than the horizontal acceptance (0.1 r) in order to severely limit beam halos and to obtain another constraint on the decay vertex position. Downstream of the final beam collimator is a 4 m long decay region which is surrounded by the main detector. Approximately 16% of the kaons decay yielding a decay rate of about 14 MHz. The beam region is evacuated to a level of 10^{-7} torr to suppress neutron-induced π^0 production in the residual gas. The decay region is surrounded by an efficient Pb/scintillator photon veto detector ("barrel veto"). In order to simplify triggering and off-line analysis, only events with the signature of a single kaon decay producing two photons occurring within the period between microbunches are accepted.

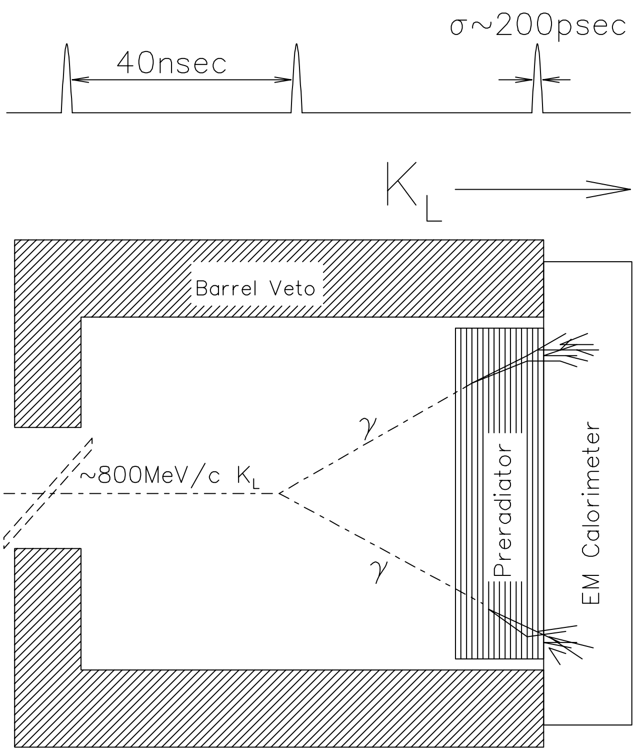

Fig. 25. Elements of the KOPIO concept: a pulsed primary beam produces low energy kaons whose time of flight reveals their momentum when the π^0 from $K_L^0 \to \pi^0\nu\bar{\nu}$ decay is reconstructed.

Photons from $K_L^0 \to \pi^0\nu\bar{\nu}$ decay are observed in a two-stage endcap detector comprised of a fine-grained preradiator followed by an 18-radiation-length (X_0) electromagnetic calorimeter. The preradiator obtains the times, positions and angles of the interacting photons from π^0 decay by determining the initial trajectories of the first e^+e^- pairs. The preradiator consists of 64 0.034 X_0 thick layers, each with plastic scintillator, converter and dual coordinate drift chamber, for a total effective thickness of 2 X_0.

The calorimeter behind the preradiator consists of "shashlik" modules, roughly 10 cm by 10 cm in cross section and 18 X_0 in depth. A shashlik module consists of a stack of square tiles with alternating layers of Pb and plastic scintillator read out by penetrating wavelength shifter (WLS) fibres. The preradiator-calorimeter combination is expected to have an energy resolution of $\sigma_E/E \simeq 0.033/\sqrt{E}$.

Suppression of most backgrounds is provided by the hermetic high efficiency charged-particle and photon detector barrel veto. This system includes scintillators inside the vacuum chamber, decay-volume photon veto detectors and veto detectors downstream of the main decay volume. The barrel veto detectors are constructed of Pb/scintillator sandwiches providing about 18 X_0 for photon conversion and detection. The downstream section of the veto system is needed to reject events where photons or charged particles escape the decay volume through the beam hole. It consists of a sweeping magnet with a horizontal field, scintillators to detect charged particles deflected out of the beam, and photon veto modules. A special group of Čerenkov radiators – the "catcher" – vetoes particles that remain in the beam phase space. This system takes advantage of the low energy nature of our environment to provide the requisite veto efficiency while being blind to the neutrons and K^0s in the beam.

TRIUMF's role

The main contribution of the Canadian group is proposed to be the KOPIO preradiator detector. Each preradiator layer consists of a flat square-cell drift chamber based on an extruded Al comb backplane, and an extruded scintillator read out using WLS fibres. The preradiator position measurements are obtained from cathode strips in the drift chambers running perpendicular to the wires. Prototype chambers are under construction and a preliminary design has already been used to successfully establish the functionality for photon pointing in beam tests at the BNL LEGS by KOPIO collaborators at Yale University. A scheme for the analogue electronics for the cathode strips has been developed using on-board front-end amplifiers, ADCs and programmable logic devices. The timing electronics is based on front-end chips which include the preamp and a programmable discriminator followed by an ASIC developed for PHENIX and ATLAS muon chambers with a tapped delay line for the drift time measurement. The entire preradiator will consist of 64 layers with a total of approximately 80,000 wires with timing readout, 80,000 strips with analogue readout, and 840 phototubes for the scintillator layers.

The HERMES experiment

(C.A. Miller, M.C. Vetterli, TRIUMF; M.G. Vincter, Alberta)

More than a decade ago, the HERMES experiment was conceived as a comprehensive and concise investigation of the spin structure of the nucleon. It was designed with unique capabilities to produce data that were not possible with previous measurements at SLAC, CERN, and Fermilab. Most prominently, it combines pure nuclear-polarized atomic gas targets in a high-energy stored polarized electron beam, with a large acceptance spectrometer to detect hadrons associated with the scattered electron. Since the commissioning in 1995, the collaboration has collected and analyzed millions of deep-inelastic scattering (DIS) events using longitudinally polarized electrons and positrons incident on longitudinally polarized internal gas targets of ^{1}H, ^{2}H, and ^{3}He. Much thicker unpolarized gas targets have also been used to study certain single-spin asymmetries for the first time, as well as novel QCD effects in the nuclear environment. These data together with large sets of photoproduction events have yielded several results that were unexpected and are provoking new work, both theoretical and experimental.

Productivity of 2000 running

January–September, 2000 was a golden year for both the HERA accelerator and for HERMES. The performance and reliability of the accelerator was outstanding. Both the integrated luminosity and the beam polarization were high. Furthermore, there were no serious beam losses in the region of the HERMES target cell, resulting in continuous use of one high-quality small-aperture cell throughout the year, with high deuteron polarization and low molecular recombination. The effective polarized target thickness was almost a factor of two larger than in previous years.

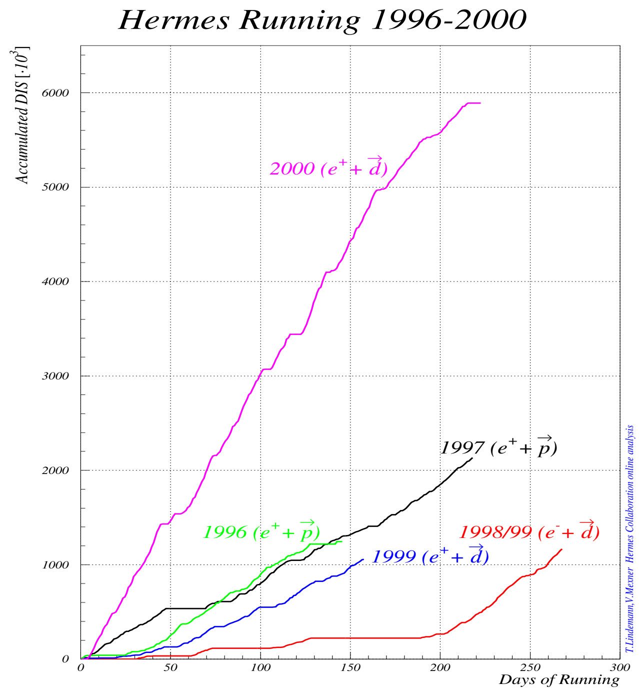

Fig. 26. Comparison of the productivity of the various running years in terms of million DIS events with polarized targets.

Figure 26 compares the accumulated number of DIS events with that of previous years.

In 2000, a new HERA operating mode was instituted for the benefit of HERMES, at negligible cost to the collider experiments. For the last hour of each beam fill, unpolarized target gas is injected at a rate limited only by either the HERMES dead time or backgrounds in the front tracking detectors. Beam lifetimes as low as 1 hour are possible, corresponding to luminosities in the range $3 \times 10^{33}\,\mathrm{cm}^{-2}\mathrm{s}^{-1}$. Such data with unpolarized targets but polarized beam are useful for several aspects of the spin physics program, especially the new study of hard exclusive processes.

Research results

The HERMES physics program has evolved to cover a broad range of topics. Here we offer a few highlights of the past year.

Polarized quark distributions

The modern generation of DIS experiments has done much to unravel the polarizations of the three flavours of valence and sea quarks, especially the controversial strange sea. However, a key limitation of inclusive DIS measurements is that they are sensitive only to linear combinations of quark flavours weighted by the *squares* of their charges, and hence can't distinguish quarks from anti-quarks. A technique that can distinguish the polarizations of anti-quarks is semi-inclusive DIS, where the flavour of the struck quark is statistically "tagged" by a hadron h detected in coincidence with the scattered lepton. This technique has been applied by both SMC and HERMES, with only limited success up to now mainly because of the limitations of the published semi-inclusive data on the neutron. However, this situation is changing radically as analysis proceeds on the 1999/2000 HERMES data set on the deuteron, which complements the large 1996/97 proton data set. An impression of this impact is given by the preliminary result of an analysis including only data recorded up to the end of 1999, and without yet making use of the new RICH detector to distinguish kaons from pions. Figure 27 shows preliminary polarized quark distributions extracted from these combined inclusive and semi-inclusive DIS data. When all the data in hand are analyzed, it is expected that the statistical error bars will become negligible for all but those for the strange sea, which are expected to be smaller than those shown in Fig. 27 for $\Delta\bar{u}$.

Hard exclusive processes

As recently as 5 years ago, one aspect of the nucleon spin puzzle threatened to remain clouded in mystery. No practical experimental access to the *orbital* angular momenta of partons had been identified. However, a seminal paper by X. Ji led to an explosion of theoretical activity, and the recent appearance of intriguing

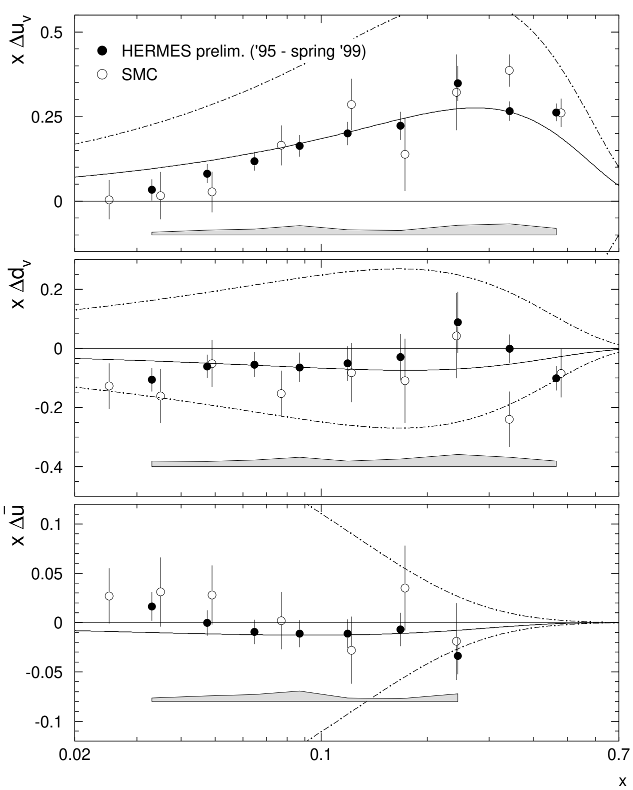

Fig. 27. Polarized quark distributions from 1995–1999 HERMES data.

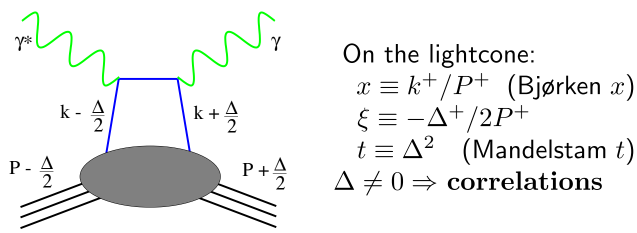

Fig. 28. Feynman ("handbag") diagram for DVCS.

new data. This paper demonstrated that the so-called generalized or "skewed" parton distributions (SPDs) embody information about parton orbital angular momentum, and that information about this could be extracted from exclusive processes such as deeply virtual Compton scattering (DVCS), illustrated in Fig. 28.

There are four SPDs, two of which appear in inclusive DIS – the unpolarized function $H(x,\xi,t)$ and the polarized one $\tilde{H}(x,\xi,t)$. In the forward limit, they reduce to familiar distributions:

$$\begin{aligned} q(x) &= H^q(x,\xi=0,t=0), \quad \text{and} \\ \Delta q(x) &= \tilde{H}^q(x,\xi=0,t=0). \end{aligned}$$

Two analogous functions are associated with target helicity flip and appear experimentally only at finite t: $E(x,\xi,t)$ and $\tilde{E}(x,\xi,t)$. Although they are all functions of three variables, their behaviour is strongly constrained by symmetry principles – e.g. their first x-moments are independent of ξ and are connected with elastic form factors.

Of primary interest to us is the "Ji sum rule" that relates their second moments to *total* (including *orbital*) quark angular momentum:

$$\begin{aligned} J^q &= \frac{1}{2}\Delta\Sigma + L^q \\ &= \frac{1}{2}\int_{-1}^{1} x\ dx\ \left[H^q(x,\xi,t=0) + E^q(x,\xi,t=0)\right]. \end{aligned}$$

It is the second term involving E^q to which experimental access is difficult. It must be measured at finite t and extrapolated to the forward limit. Another apparent obstacle is a large background contribution from the indistinguishable Bethe-Heitler process – radiative "elastic" lepton-proton scattering. However, this can be turned to advantage. Interference between the two processes provides direct experimental access to the DVCS amplitudes by giving rise to large asymmetries in the azimuthal distribution of the detected photons about the direction of the incident virtual photon. These asymmetries are associated with, e.g., the beam lepton charge, and also in some cases with its polarization. Furthermore, each of several different moments of these azimuthal asymmetries is associated with a particular linear combination of DVCS amplitudes in the interference cross section.

HERMES kinematics are ideal for observing the DVCS/Bethe-Heitler interference. Figure 29 shows the first measurement of lepton beam spin asymmetries in the azimuthal distribution of photons, in leptoproduction from an (unpolarized) hydrogen target. In the vicinity of $M_X = M_\mathrm{p}$, the observed $\sin\phi$ moment of the asymmetry is large, as predicted. Several other observables can be expected to emerge soon from HERMES data, for both DVCS and exclusive production of various mesons. A recoil detector to identify truly exclusive final states is under development. This field is still in its infancy, and a large program will be needed to understand and disentangle the SPDs. Transverse target polarization is expected to be particularly fruitful. Each measurement constrains only a moment of one or more functions, along a trajectory in the 3-dimensional kinematic space. Exclusive meson production by longitudinal photons can provide independent constraints. HERMES is in a good position to lead the present exploratory phase.

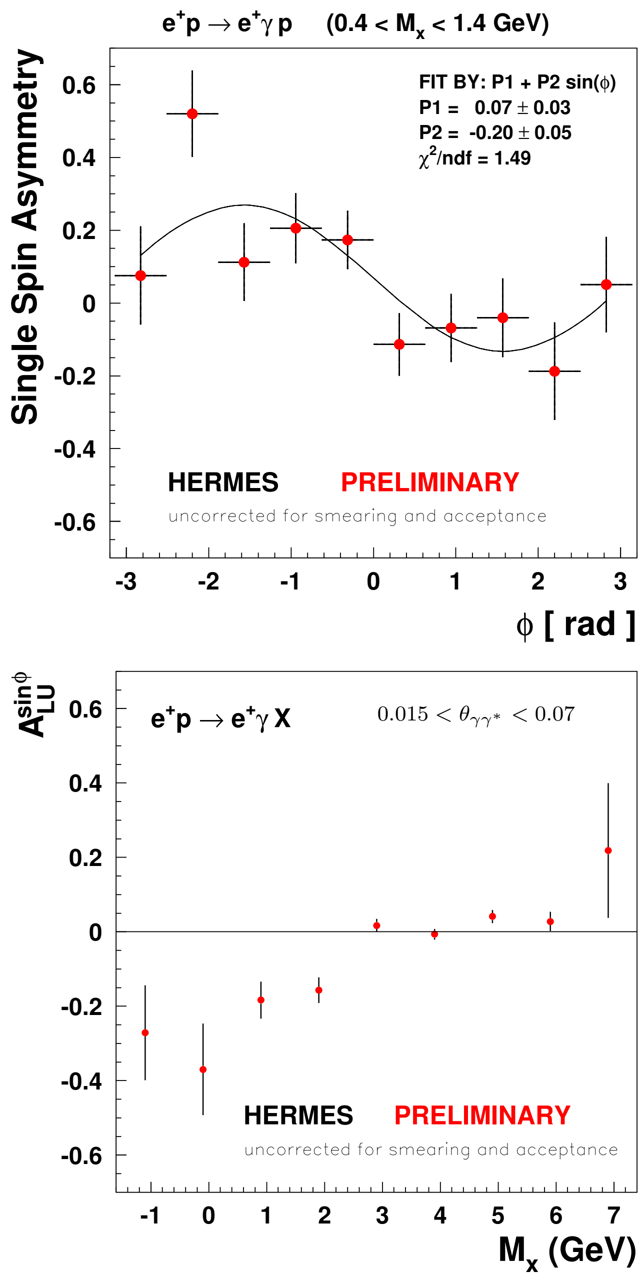

Fig. 29. Lepton beam spin asymmetries in the azimuthal distribution of photons produced semi-exclusively from an unpolarized hydrogen target.

Hadron formation times

In deep-inelastic scattering (DIS), an incident lepton interacts with a target via the exchange of a gauge boson between the lepton and a parton (a quark or an anti-quark). The struck parton is subjected to a sequence of hard parton- and soft hadron-production processes, resulting in the formation of hadrons. By carrying out DIS experiments on nuclear targets, it is possible to study the hadronization process during the time period immediately after the quark has been struck by the virtual photon. In the simplest scenario the nucleus, which has the size of a few fm, acts as an ensemble of targets with which the struck quark or the produced hadron may interact. If an interaction occurs, the number of leading hadrons produced per DIS event and per nucleon is reduced compared to that for a free nucleon. The reduction of hadron multiplicity depends on the distance traversed by the struck quark before the hadron is formed, the (unknown) quark-nucleon cross section and the (known) hadron-nucleon cross section. Hence, measurements of the multiplicity of hadrons produced on nuclei can provide information on the space-time structure of the hadronization process.

The differential multiplicity of charged hadrons and identified charged pions from nitrogen relative to that from deuterium has been measured as a function of the virtual photon energy ν and the fraction z of this energy transferred to the hadron. The results are much more precise than previous such data. There are observed substantial reductions of the multiplicity ratio R_M^h at small ν and at large z, both of which are well described by a gluon-bremsstrahlung model of hadronization, as shown in Fig. 30. The effect at large z is observed here for the first time, and is inconsistent with simple phenomenological models. A significant difference of the ν-dependence of R_M^h is found between positive and negative hadrons. This is interpreted in terms of a difference between the formation times of protons and pions, using a phenomenological model to describe the ν- and z-dependence of R_M^h.

Outlook

The HERMES collaboration intends to continue recording data in the years 2001–2006, i.e., after the

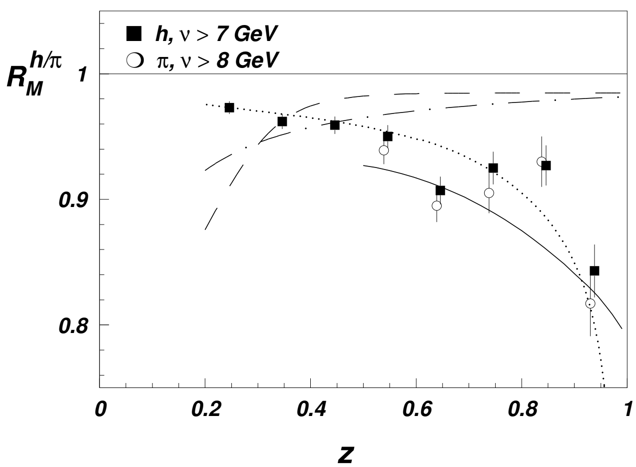

Fig. 30. The multiplicity ratio as a function of z for all charged pions (open circles) and all charged hadrons including pions (closed squares). The full curve represents a gluon-bremsstrahlung model calculation for pions. The dotted, dashed and dot-dashed curves represent phenomenological formation-time calculations, the latter with an *ad hoc* z-dependence.

HERA luminosity upgrade, as many important (and often unique) measurements can be made concerning the (spin) structure of the nucleon and related areas. The most prominent measurements foreseen include: (1) the transverse polarization of quarks, (2) the longitudinal polarization of gluons, (3) the longitudinal polarization of strange quarks, and (4) constraints on generalized or skewed parton distributions that can eventually shed light on the *orbital* angular momenta of partons. In some cases, the new measurements will enhance the precision of results already obtained at HERMES in the past years.

HERA is in a long shutdown from October, 2000 to summer, 2001 for the collider luminosity upgrade. During this time, HERMES is installing a transversely-polarized proton target with the purpose of making the first measurement of transversity, the only remaining unmeasured one of the three most fundamental (leading twist) flavour-sets of parton distribution functions. Furthermore, a wheel-shaped array of silicon counters is being installed just downstream of the target such that the acceptance for Λ^0 hyperons and J/ψ mesons (in conjunction with new wide-angle scintillators behind the magnet) will be increased by a factor of four. It is now planned to spend the next two years of running for the measurement of transversity, together with certain critical observables in exclusive processes.

HERMES collaborators include: H. Coombes, L. De Nardo, P. Green, L.G. Greeniaus, P. Kitching, G. Kotik, B. Seitz, M.G. Vincter (Univ. of Alberta); L. Felawka, M. Hartig, C.A. Miller, R. Openshaw, J. Stewart, M.C. Vetterli, S. Yen (TRIUMF); J. Wendland (Simon Fraser Univ.).

KEK Expt. 246 (Japan-Russia-Canada-Korea-U.S.A. Collaboration)
Search for T-violation in $K_{\mu 3}$ decay
(M.D. Hasinoff, UBC.; J.A. Macdonald, B. Shin, TRIUMF)

Measurement of the muon transverse polarization, P_T, in the decays $K^+ \to \pi^0\mu^+\nu$ ($K_{\mu 3}$) and $K^+ \to \mu^+\nu\gamma$ ($K_{\mu 2\gamma}$) can provide important insight to new physics beyond the standard model (SM). In $K_{\mu 3}$ decay, P_T is a T-odd observable $\mathbf{s}_\mu \cdot (\mathbf{p}_\pi \times \mathbf{p}_\mu)$ determined by the π^0 momentum $\mathbf{p}_\pi$ and the muon momentum $\mathbf{p}_\mu$ and spin $\mathbf{s}_\mu$. In $K_{\mu 2\gamma}$ decay, P_T is proportional to $\mathbf{s}_\mu \cdot (\mathbf{q} \times \mathbf{p}_\mu)$, where $\mathbf{q}$ is the photon momentum. These observables are predicted to be very small in the SM [Golovich and Valencia, Phys. Rev. **D40**, 112 (1989)], so they can be interesting probes of non-SM CP-violation mechanisms [Garisto and Kane, Phys. Rev. **D44**, 2038 (1991); Fabbrichesi and Vissani, Phys. Rev. **D55**, 5334 (1997); Wu and Ng, Phys. Lett. **B392**, 93 (1997); Bélanger and Geng, Phys. Rev. **D44**, 2789 (1991); Kobayashi *et al.*, Prog. Theor. Phys. **95**, 361 (1995)] where P_T could be as large as 10^{-3} in either $K_{\mu 3}$ or $K_{\mu 2\gamma}$.

Whether CP or T is violated or not, a non-vanishing P_T in both decays can be induced by electromagnetic final-state interactions (FSI). The value of P_T due to the FSI is expected to be about 4×10^{-6} for $K_{\mu 3}$ decay, i.e., much smaller than the expected non-SM effects. However, for $K_{\mu 2\gamma}$ decay, the FSI can induce a P_T up to 10^{-3} [Efrosinin and Kudenko, Yad. Fiz. **62**, 1054 (1999)] depending on the values of the axial vector form factor F_A and the vector form factor F_V. Moreover, P_T varies significantly over the Dalitz plot, reaching a maximum value of $10^{-3} - 10^{-2}$ at large muon energies, i.e., in the region of high sensitivity to T-violating parameters.

In 1999, after the analysis of data taken in 1996 and 1997, we reported a value for P_T in $K_{\mu 3}$ of $-0.0042 \pm 0.0049(stat) \pm 0.0009(\mathrm{syst})$ and $\mathrm{Im}(\xi) = -0.013 \pm 0.016(\mathrm{stat}) \pm 0.003(\mathrm{syst})$ [Abe *et al.*, Phys. Rev. Lett. **83**, 4253 (1999)]. During 2000 we obtained the final data set and we have now completed the analysis of the 1998 data. The results continue to be consistent with zero transverse muon polarization. The statistical error of P_T for the combined 1996-98 result is expected to be about 3×10^{-3} (1σ level) which corresponds to $\delta\mathrm{Im}(\xi) \sim 1.1 \times 10^{-2}$. The final KEK Expt. 246 sensitivity to P_T in $K_{\mu 3}$ is expected to be $\sim 2 \times 10^{-3}$ corresponding to $\delta\mathrm{Im}(\xi)$ of about 7×10^{-3}. The systematic error will be one third the statistical error. Since statistics mainly determine the sensitivity, the detector still has a capability to improve the sensitivity at least by a factor of 3–4 using a more intense kaon beam.

Including our final run in 2000, we expect to accumulate $(2-3)\times 10^5$ "good" $K_{\mu 2\gamma}$ events. The final sensitivity to T-odd muon polarization in $K_{\mu 2\gamma}$ decay is expected to be at the level of about 1.5×10^{-2}.

In addition to the polarimeter experiments, the KEK Expt. 246 apparatus has been used to study other physics of K decays. In 2000, results were published based on the decays $K^+ \to \pi^+\pi^0\pi^0$ ($K^+_{\pi 3}$) [Shin *et al.*, Eur. Phys. J. **C12**, 627 (2000)] and $K^+ \to \pi^0 e^+ \nu_\mu$ (K_{e3}) [Shimizu *et al.*, Phys. Lett. **B495**, 33 (2000)].

The matrix element of $K^+_{\pi 3}$ can be expanded [Weinberg, Phys. Rev. Lett. **4**, 87 (1960)] to lowest order in s_i as:

$$|M|^2 \sim 1 + gY + hY^2 + jX + kX^2....$$

where $Y = (s_3 - s_0)/m^2_{\pi^+}$, $X = (s_1 - s_2)/m^2_{\pi^+}$ with $s_i = (M_K - M_i)^2 - 2M_k T_i$ and $s_0 = (M_K^2 + 2M^2_{\pi^0} + M^2_{\pi^+})/3$, $g = 0.594 \pm 0.0219$ and $h = 0.035 \pm 0.015$. In the present experiment both π^0s can be reconstructed; hence the values j and k can be determined for the first time. j should be zero if CP invariance holds. If CP violation is present, it should be about –3.3 times the value observed in $K^+ \to \pi^+\pi^+\pi^-$. The coefficients h and k provide information on whether the final state contains more than one state of isospin, and thus provide a test of the $\Delta I = 1/2$ rule, which states that $\Delta I = 1/2$ transitions are dominant in kaon decays. The confirmation of this rule stems from the ratio of branching ratios, $\frac{\Gamma(\pi^0\pi^0\pi^+)}{\Gamma(\pi^+\pi^+\pi^-)}$, which proves $\Delta I = 5/2$ and $\Delta I = 7/2$ are absent but nothing about the presence of $\Delta I = 3/2$ terms, which may arise from a $\Delta I = 1/2$ strangeness-nonconserving current. In this experiment we have determined the following values: $g = 0.518 \pm 0.039$ and $k = 0.043 \pm 0.020$. Hence the quadratic term in $(s_2 - s_1)$ is small but nonzero, and the new world average value for g becomes $g = 0.587 \pm 0.019$, in excellent agreement with the value $g = 0.582 \pm 0.021$ for the CP symmetry partner $K^- \to \pi^-\pi^0\pi^0$. Furthermore, the $\Delta I = 1/2$ rule seems to be violated since the prediction for g_{+00} is 0.43 using $g_{++-} = -0.2154 \pm 0.004$ and $g_{--+} = -0.217 \pm 0.010$.

This kinematically complete experiment also allows a nearly model independent determination of both the isoscalar and isotensor $\pi - \pi$ scattering lengths free from the usual problems caused by the final state hadronic and Coulomb interactions. Our measured values lead to a value for the Weinberg parameter in nearly perfect agreement with the value $W = 0.56$ currently predicted by the Goldberger-Treiman relation.

The semi-leptonic K_{e3} decay proceeds via W exchange in the SM with pure $V-A$ coupling. However, a previous in-flight K^+-decay experiment [Akimenko *et al.*, Phys. Lett. **B259**, 225 (1991)] reported anomalous scalar and tensor couplings, as did a KTeV result [Tesarek, hep-ex/9903069 (1999)] from neutral K_{e3}. The existence of these exotic couplings is in distinct disagreement with the SM and requires an acurate experimental check.

Using the KEK Expt. 246 apparatus with its high degree of control over systematic effects, we were able to obtain clean samples of K^+_{e3} decays using the toroidal spectrometer at two values of the magnetic field to analyze e^+'s, and the CsI(Tl) array to measure the π^0's. Selection criteria on time of flight, two-photon invariant mass and $e^+ - \pi^0$ opening angle were the main strategies used to reject the major backgrounds to less than 0.3% of the total 4×10^4 K^+_{e3} events.

The Dalitz plot of the selected events was then fit to the theoretical Dalitz plot derived using the general Lorentz invariant form of the matrix element, with the potential scalar, f_S, and tensor, f_T, coupling strengths and the q-dependence, λ_+, of the vector coupling as parameters. When the pure $V-A$ form is assumed, λ_+ is the only free parameter. It was found that the value of λ_+ was consistent with the world average, with or without the inclusion of exotic couplings, and that the values of f_S and f_T were consistent with pure $V-A$ coupling, in contrast to the previous experiments.

TJNAF Experiment E00-006
Measurement of the flavour singlet form factors of the proton ($G\emptyset$)

(W.T.H. van Oers, Manitoba)

The structure of the nucleon at low energies in terms of the quark and gluon degrees of freedom is not well understood. The $G\emptyset$ experiment is to measure two proton ground state matrix elements which are sensitive to point-like strange quarks and hence to the quark-antiquark sea in the proton. The matrix elements of interest are the elastic scattering vector weak neutral current charge and magnetic form factors, G_E^Z and G_M^Z, respectively. These can be extracted from a set of parity-violating electron-proton scattering measurements. If one assumes a relationship between the proton and neutron structure in that the proton and neutron differ only by the interchange of up and down quarks, i.e., isospin symmetry, the strange quark (as well as the up and down quark) contribution to the charge and magnetic form factors of the nucleon can be determined. This would result from taking appropriate linear combinations of the weak neutral form factors and their electromagnetic counterparts.

Determinations of both the charge and magnetic strange quark form factors are of fundamental interest, as these would constitute the first direct evidence of the quark sea in low energy observables. It is the objective of the $G\emptyset$ experiment to determine these contributions to the proton form factors at the few percent level. Observations at high energy suggest that the strange quarks carry about half as much momentum as the up and down quarks in the sea. It is important to determine both the role of the quark sea and the relevance of strange quarks at low energy where there are voids in understanding the theory of the strong interaction (quantum chromodynamics, QCD). Even if the strange quark contributions do not amount to the level of sensitivity of the experiment, upper limit determinations at this level are as valuable as non-zero results. The matrix elements, G_E^Z and G_M^Z, are also relevant to discussions of the Ellis-Jaffe sum rule and the pion-nucleon sigma term; there is uncertainty in both of these about the strange quark contributions. The $G\emptyset$ experiment will allow the determination of the strange contributions to the proton charge and magnetic form factors in a much more straightforward manner than is possible with regard to the corresponding observables in the above two deduced relations.

In the $G\emptyset$ experiment, parity-violating longitudinal analyzing powers will be measured in electron-proton scattering in the range $0.1 \leq Q^2 \leq 1.0\,\mathrm{GeV}^2$ at both forward and backward angles. The longitudinal analyzing power is defined as

$$A_z = (1/P)\frac{[\sigma^+(\theta) - \sigma^-(\theta)]}{[\sigma^+(\theta) + \sigma^-(\theta)]}$$

where P is the polarization of the incident electron beam and the $+$ and $-$ signs indicate the helicity state. Making pairs of measurements at forward and backward angles will allow the separation of G_E^Z and G_M^Z. Predicted longitudinal analyzing powers range from about (–3 to 35) $\times\ 10^{-6}$; it is planned to measure the longitudinal analyzing powers with statistical uncertainties of $\Delta A/A = 5\%$ and systematic uncertainties related to helicity correlated effects of $\Delta A \leq 2.5 \times 10^{-7}$. In the first phase of the experiment longitudinal analyzing powers will be measured concurrently at seven values of the momentum transfer in the range $0.1 \leq Q^2 \leq 1.0$ GeV^2. It now appears highly probable that by the time of data-taking for the $G\emptyset$ experiment (starting in 2002) higher beam polarizations ($\sim$70%) will also be available at the reduced beam pulse frequency of 31 MHz, decreasing considerably the original estimate of 700 hours for the first phase of the experiment. However, it must be realized that the length of the experiment is in part governed by making rather elaborate control measurements to determine the corrections that have to be made to the measured asymmetries and to assess systematic errors. In the second phase of the experiment each subsequent backward angle analyzing power measurement would require from one half to one month of running time. The results of the SAMPLE experiment at the MIT-Bates Laboratory have shown the importance of measuring the axial form factor corrections, since these appear to be quite different from the theoretical predictions. Therefore, companion measurements of quasi-elastic scattering from deuterium will also be made at the backward angles (to be proposed at a future Program Advisory Committee meeting). With these measurements, the effective axial current of the nucleon will also be determined. This current includes effects from the effective axial coupling of the photon to the nucleon or anapole moment, which are relevant also in other processes, e.g., parity violating Moller scattering and atomic parity violation.

The $G\emptyset$ collaboration

The $G\emptyset$ experiment will be carried out in Hall C at TJNAF by a collaboration of scientists from Canada, France, Georgia, and the United States, with funding provided through NSERC (Canada), IN2P3 (France), and DOE/NSF (US).

Canadian contributions

The Canadian members of the $G\emptyset$ collaboration, based at the universities of Manitoba and Northern British Columbia, and TRIUMF, have been asked to: (i) develop and produce specialized photomultiplier tube bases for the main detector arrays; (ii) prototype and produce the cryostat exit detector arrays for the backward angle measurements; (iii) prototype and produce the Aerogel Čerenkov arrays for background rejection in the backward angle measurements; (iv) coordinate the implementation of TJNAF built specialized beam monitors and control apparatus, and TRIUMF built parity-type electronics to read out these monitors on the Hall C beam line; (v) design, build, and test an automated magnetic field measuring apparatus complete with its own data acquisition system; and (vi) devise a set of measurements to determine the neutron background to which the $G\emptyset$ detector system will be subjected. Much progress has been made in the designing and building of the various subsystems listed above.

The $G\emptyset$ main detector array

The heart of the $G\emptyset$ detection system is a spectrometer which consists of an eight-sector toroidal magnet, with an array of scintillation detectors located at the focal surface of each sector (see Fig. 31). Since data will not be acquired in event-by-event mode in this experiment, and the scintillator arrays are the only detectors to measure the scattered particles in the forward angle mode, the performance of these focal-plane detectors (FPD) is of critical importance. The timing and pulse shape characteristics of this system must be fine-tuned at the hardware level as it will not be possible to reconstruct individual events. Furthermore, the rates associated with many of the FPD elements

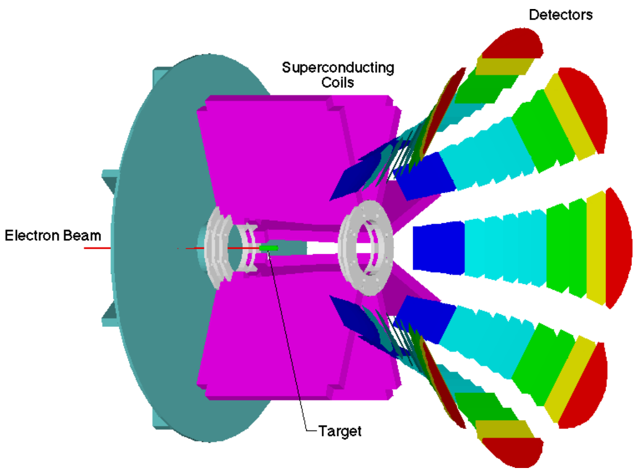

Fig. 31. View of the $G\emptyset$ superconducting toroidal spectrometer with one sector and the housing removed.

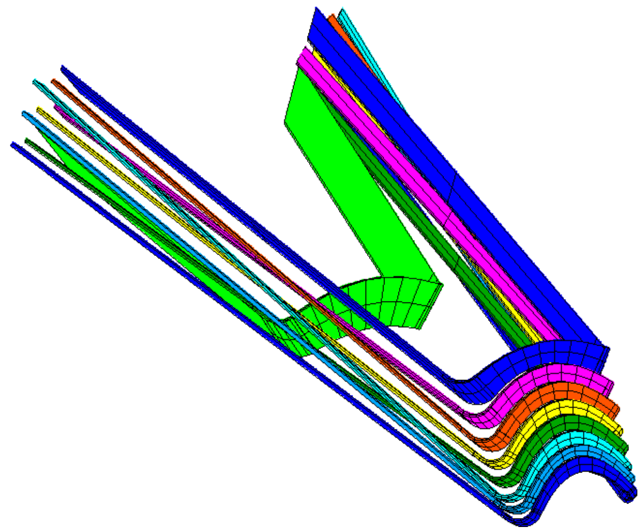
Fig. 32. Geometry of the cryostat exit detector (CED) array for a single octant.

will be quite high (1 MHz) and the photon yield(s) will have a large dynamic range. As such, very special demands will be made on the photomultiplier tubes (PMT) and especially on their associated divider/base circuit. Much progress has been made in the design, development, and building of the $G\emptyset$ bases at TRIUMF. Several iterations of prototype high-rates bases were constructed and tested in late 1997 and early 1998. In the summer of 1998, 12 final prototype bases were constructed and delivered to TJNAF for tests with the first set of prototype FPDs, and fabrication of the production bases began. With the help of summer students (funded partly through the TRIUMF Summer Students program and partly through the $G\emptyset$ NSERC grant), the fabrication of the electrical components for all of the production bases was completed in late summer, 1998. The design of the mechanical housing for the PMT-base subsystem depended on the final design of the FPD support structure and, after much effort resolving subsystem integration issues, the final design for the PMT-base housing assembly was completed in late 1998. The fabrication and assembly of the mechanical housings and integration of the electrical components was completed over the summer of 1999 (again with the help of summer students at TRIUMF). Final testing of the completed bases was carried out in late fall, 1999, and shipment of all the bases (300 units) to TJNAF occurred at the end of calendar year 1999. The remaining task for this subsystem, integration with the FPD arrays and the DAQ electronics, is presently being carried out at TJNAF as assembly of the FPD system proceeds.

The cryostat exit detector array

For the backward angle measurements during the second phase of the $G\emptyset$ experiment, simulation results have shown that the addition of a second array of scintillation detectors, located near the spectrometer-cryostat exit windows, will be required in order to separate the elastic and inelastic electrons. The geometry of these cryostat exit detector (CED) arrays has been studied in detail (see Fig. 32), and a reference design was completed in the spring of 1999. Due to the resident expertise at TRIUMF in producing high quality scintillation detectors and lightguides, the Canadian subgroup has been asked to play the main role in the prototyping and production of the CEDs. A set of prototypes was built at TRIUMF and delivered to Louisiana Tech University for further studies in early summer, 1999. Results from these studies indicate that the reference design and the prototype detectors will meet the specification requirements for the CED arrays. Upon finalizing the CED design in the summer, production of a set of final blank prototype detectors was completed at TRIUMF and delivery made to Louisiana Tech University for assembly tests with the CED support structure. Construction of the CEDs started at TRIUMF in late 2000 and will continue on into 2001. The CEDs will also make use of the same photomultiplier tubes and specialized TRIUMF/$G\emptyset$ bases as the FPDs.

Aerogel Čerenkov array

Recent Monte Carlo simulation results have shown that backgrounds due to negative pions will be problematic for the second phase backward angle measurements. Present efforts of the $G\emptyset$ Simulation subgroup (which includes members of the Canadian subgroup) include studying and characterizing this π^- background and providing options regarding the design of a set of veto detectors. The $G\emptyset$ Canadian subgroup has been asked to undertake the prototyping and construction of this crucial set of veto detectors, which will be made up of arrays of Aerogel Čerenkov counters. A conceptual design is shown in Fig. 33.

Fig. 33. Conceptual layout of the Aerogel Čerenkov veto detector for a single octant.

Beam position and current monitors

Five sets of XYQ monitors will be required in order to measure the beam current and trajectory at several critical locations. A beam current sensitivity of $\pm\, 4 \times 10^{-5}$ measured in a 33 ms integration-time sample will be required to monitor and correct for possible helicity correlated intensity modulations. For the beam position monitors (BPM), a spatial resolution of better than 25 μm at an integration time of 33 ms will be required. The beam current and position monitors were tested during an engineering run in July, 1997 at TJNAF. The run was organized by members of the $G\emptyset$ Canadian subgroup and personnel from TJNAF (Hall C), with much of the parity-type electronics provided by the Canadian subgroup. Helicity correlated properties of the TJNAF polarized electron beam and noise characteristics of some of the beam monitors were successfully measured. Analysis of the data indicates that the beam current and position monitors will meet the specification requirements listed above. Further test beam time is planned for the future. To read out the analogue signals from the beam current and position monitors, and to provide feedback control signals, specialized parity-type electronics is required for the $G\emptyset$ experiment. Much of this electronics, such as precision analogue subtractors/dividers and precision voltage-to-frequency converters, has already been designed and used by members of the Canadian subgroup in their parity experiments at TRIUMF. Modifications, driven by $G\emptyset$ requirements, were made to some of these modules and they were operated successfully at the July, 1997 engineering run at TJNAF, as mentioned above. Since that time, several voltage-to-frequency converters of the TRIUMF/parity variety have been requested by TJNAF for the $G\emptyset$ experiment. Construction of these 32-channel precision V-to-Fs was completed at TRIUMF and delivery made to TJNAF in early 1998. With the successful implementation of these first sets of converters, a second set of V-to-F modules was requested by TJNAF in summer, 1999. This second set of V-to-F modules was again constructed at TRIUMF and delivered to TJNAF in fall, 1999. At present, a third set of V-to-F modules has been requested by TJNAF and is presently under construction at TRIUMF. It is anticipated that several more sets of V-to-F modules, as well as other specialized parity-type electronics modules, will be required by the $G\emptyset$ collaboration over the next few years as the experiment moves into the commissioning and data-taking phase.

Magnetic field measuring apparatus

An automated field measuring apparatus will be used to provide a magnetic verification of the $G\emptyset$ superconducting toroid by determining the locations of a pre-specified set of magnetic reference points. These reference points correspond to the zero-crossing locations of specific field components at selected points of symmetry around the toroidal magnet. This measurement will be carried out by scanning a predefined set of contour lines, and determining where specific field components reverse signs. The system must be capable of providing a position determination of $\pm$ 0.2 mm and a field determination of $\pm$ 0.2 G. Over the past year, considerable effort has gone into the design and construction of this magnetic field measuring apparatus or magnetic verification device at TRIUMF and the University of Manitoba (see Fig. 34). The device consists of a programmable gantry – capable of full 3D motion anywhere within a 4 m $\times$ 4 m $\times$ 2 m volume – with a set of high precision Hall probes, temperature, inclination, and photo sensors mounted at the end of a probe boom on the gantry. Procurement of parts commenced in early 2000, and assembly and testing began in late spring at TRIUMF. The magnetic verification device was completed in mid-summer and transported to the University of Illinois for final tests and commissioning. This task was carried out by members of the $G\emptyset$ Canadian subgroup and TRIUMF personnel at the University of Illinois during the fall, and will be followed by a first set of measurements on the $G\emptyset$ spectrometer in early 2001. Although this magnetic verification device is being designed, tested, and built by the Canadian subgroup at TRIUMF and the University of Manitoba, it should be noted that funding for all hardware components of this subsystem has been provided via NSF funding for $G\emptyset$ through the University of Illinois. Infrastructure support, however, has been provided by TRIUMF and the University of Manitoba.

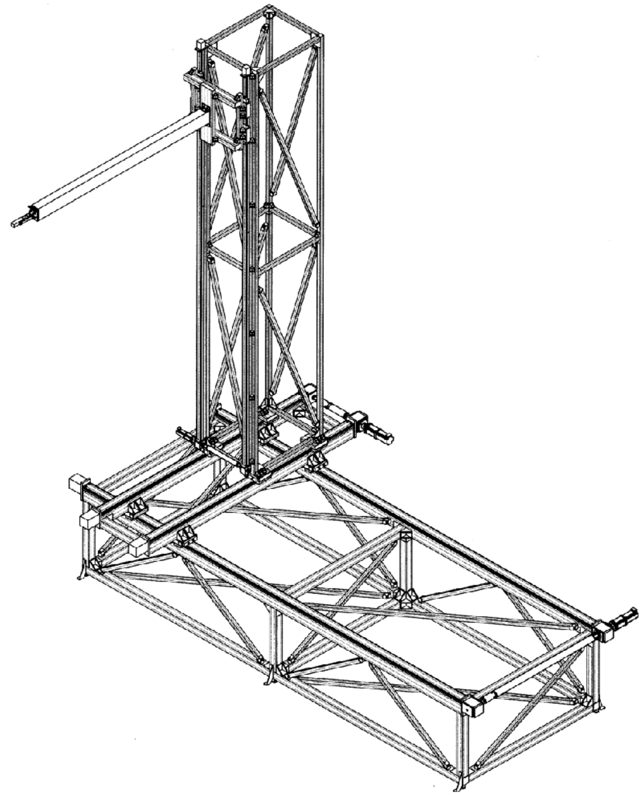

Fig. 34. Drawing of the magnetic verification device, which consists of a programmable gantry (capable of full 3D motion anywhere within a 4 m $\times$ 4 m $\times$ 2 m volume) with a set of high precision Hall probes, temperature, inclination, and photo sensors mounted at the end of a probe boom on the gantry.

Neutron background studies

A set of measurements is being devised to determine the neutron background and energy spectrum in the vicinity of the $G\emptyset$ detector system. This effort is being coordinated by the Canadian subgroup with help from members of the TRIUMF Safety group (L. Moritz and others) and personnel from TJNAF. The present set of proposed measurements makes use of a Multisphere (Bonner sphere) detector system, which is capable of determining the neutron energy spectrum at specific locations. The Multisphere detector consists of a ^{6}LiI(Eu) scintillation counter system, used in conjunction with a set of moderating polyethylene spheres. Neutron rates/yields are measured via the neutron capture reaction $^6\text{Li}(n,\alpha)t$ in the scintillator, under different moderating sphere configurations. The underlying neutron energy spectrum can then be unfolded from the set of yield measurements. Test beam time in Hall C was made available in December, 1999, and a first set of neutron background measurements using the Multisphere detector(s) was carried out. Data from this test run have been analyzed and preliminary results have been disseminated. Further test beam time is planned for the future. Presently, one Multisphere detector system exists at TRIUMF and was made available for this measurement. Current plans are to build 2 more ^{6}LiI(Eu) scintillation counters to enable the studies to be completed in a timely manner.

Canadian subgroup of the $G\emptyset$ collaboration: J. Birchall, W.R. Falk, E. Gamroth, A. Horning, C. Hynes, L. Lee, S.A. Page, W.D. Ramsay, A. Rauf, G. Rutledge, W.T.H. van Oers (Manitoba); E. Korkmaz, T. Porcelli (Northern British Columbia); C.A. Davis (TRIUMF).